IDEA PROJECT FINAL REPORT
Contract ITS- 14

IDEA Program
Transportation Research Board
National Research Council

November l0,1995

ADAPTIVE FILTERING FOR ADVANCED VEHICLE CONTROL

Laura R. Ray
Christian Brothers University
Memphis, Tennessee

The ITS-IDEA program is jointly funded by the U.S. Department of Transportation's Federal Highway Administration, National Highway Traffic Safety Administration, and Federal Railroad Administration. For information on the IDEA Program contact Dr. K Thirumalai, IDEA Program Manager, Transportation Research Board, 2101 Constitution Avenue N.W., Washington, DC 20418 (phone 202-334-3568, fax 202-334-3471).

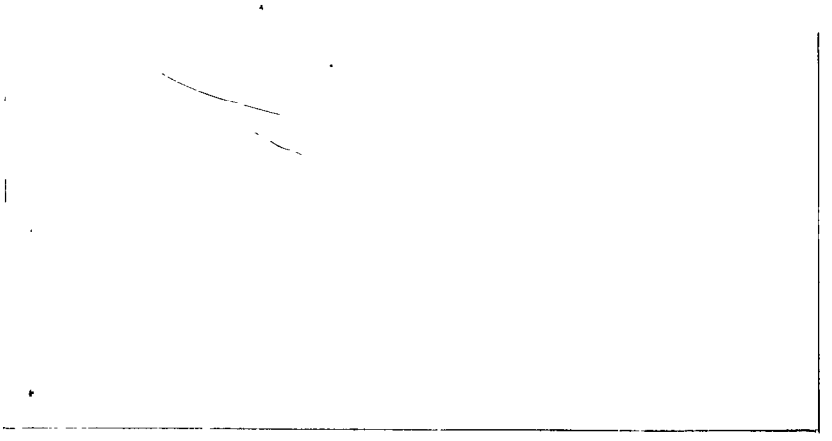

INNOVATIONS DESERVING EXPLORATORY ANALYSIS (IDEA) PROGRAMS MANAGED BY THE TRANSPORTATION RESEARCH BOARD (TRB)

This investigation was completed as part of the ITS-IDEA Program which is one of three IDEA programs managed by the Transportation Research Board (TRB) to foster innovations in surface transportation. It focuses on products and result for the development and deployment of intelligent transportation systems (ITS), in support of the U.S. Department of Transportation's national ITS program plan. The other two IDEA programs areas are Transit-IDEA, which focuses on products and results for transit practice in support of the Transit Cooperative Research Program (TCRP), and NCHRP-IDEA, which focuses on products and results for highway construction, operation, and maintenance in support of the National Cooperative Highway Research Program (NCHRP). The three IDEA program areas are integrated to achieve the development and testing of nontraditional and innovative concepts, methods and technologies, including conversion technologies from the defense, aerospace, computer, and communication sectors that are new to highway, transit, intelligent, and intermodal surface transportation systems.

TABLE OF CONTENTS

ACKNOWLEDGMENTS

The author thanks Mr. Jeff Chrstos of the National Highway Traffic Safety Administration's Vehicle Research Test Center for providing test data to complete this project. The author thanks Dr. Martin Lipinski of the Univ. of Memphis for serving as IDEA project advisor.

EXECUTIVE SUMMARY

Information required to make intelligent driving decisions depends on many factors, changes continually, and must be continually updated. Both during routine driving and emergency situations, Intelligent Transportation Systems (ITS) for automated and driver-assisted control must know whether a vehicle is capable of performing a required maneuver before implementing or proposing the maneuver; if information on which ITS decisions are based is inaccurate, the system may fail to choose the safest action Much ITS research has focused on methods of making driving decisions based on uncertain information. In addition, prior Advanced Vehicle Control System (AVCS) research has shown that feedback of signals such as wheel slip and wheel slip angle can provide significant performance gains over control systems currently used in some vehicles; however, such signals cannot be measured using current technology. This project bridges the gap between proposed ITS decision-making methods and proposed ACVS by providing numerical techniques for determining information necessary to make and implement intelligent driving decisions. The results have application to ITS products for automated driving, emergency intervention, and driver safety aids. In addition, the numerical techniques provide feedback signals that make implementation of AVCS feasible. This study demonstrates that attention to the accuracy of decision information can result in superior ITS and AVCS system performance.

A crucial parameter governing vehicle motion is the tire/road-surface coefficient of friction. Vehicle stopping distance, safe following distance, safe speed, and lateral maneuverability all depend on this uncontrollable parameter. Road friction governs the tire forces, or forces that cause deceleration and traction and that prevent a vehicle from "spinning" during a panic maneuver. While other important parameters governing vehicle motion can be measured using transducers, there is currently no method to measure or otherwise determine road friction. In the absence of a "road fiction sensor", this project aims to estimate road friction based on measured vehicle motion. Figure 1 shows a conceptual block diagram in which road friction and resulting decision and control parameters are estimated for ITS decision logic and AVCS. The major components of this project appearing inside the dotted lines include a set of transducers, an Extended Kalman Filter (EIW), a Bayesian Hypothesis Selection algorithm, and a Vehicle Parameter Determination block. The EKF provides feedback signals that can be used in braking and tractive control systems. The filter outputs also include tire force estimates that are used in the Hypothesis Selection procedure to estimate road friction from a set of possible values ranging from 0.25 (icy road) to 0.9 (dry asphalt). Road friction and vehicle motion are used in the Vehicle Parameter Determination block to predict decision parameters. Decision logic can then be used to command steering, braking, and throttle inputs that enact the vehicle control systems.

The IDEA investigation described here is a feasibility study conducted to develop and validate the EKF and Bayesian Hypothesis Selection algorithms using both computer simulation and field test data. For the simulation study, noisy transducer measurements are constructed from simulated vehicle motion. These measurements serve as inputs to the EKF. Performance of the algorithms is assessed by comparing simulated vehicle motion and true road coefficient of friction to estimates of these variables for a variety of vehicle steering and braking inputs. Results of this task demonstrate excellent tracking ability of the EKF and Hypothesis Selection procedure for a broad range of simulated vehicle inputs and road conditions. Figures 2 and 3 show example results of the EKF and road friction identification, respectively, for a panic braking and steering maneuver on a variable friction road surface similar to what may be encountered on a cold, icy day. Tracking ability of the EKF is excellent (Figure 2) and the road friction identification procedure responds nearly instantly to sudden changes in road conditions (Figure 3). The study proved the EKF to be robust to reasonably expected uncertainty in vehicle load, tire modeling, and center-of-gravity location, and worst-case error in the road friction estimate when modeling uncertainties were assumed was 0.10. Example decision parameters, such as stopping distance and brake power required to achieve a target speed were determined from road friction along with typical uncertainties in these parameters. Performance benefits of proposed AVCS were assessed by simulation as well. A simulated slip control braking system showed straight-line stopping distances up to 25% lower than a vehicle

Field test data provide a low-cost method of verifying results of the simulation studies. Example EKF and road friction identification results from processing field test data are shown in Figure 4. Figures 2 and 3 show algorithm performance for severe inputs. It is necessary that the algorithms also perform well for modest steering and braking inputs that are encountered during normal driving. Figure 4 shows road friction estimates and longitudinal force estimates from field test data for a 0.37g straight line braking maneuver from 55 mph on a dry road surface. The same maneuver was simulated on a road surface with $p = 0.88$. Consistency between simulation and test data results and known typical values of road friction for dry asphalt indicate that road friction identified is reasonable for the test track surface. The ability to process field test data collected from on-board transducers demonstrates that current sensing technology can be used to implement the algorithms developed.

The conceptual IDEA product represented in Figure 1 includes on-board transducers and a microcomputer. Required transducers include four wheel angular velocity tachometers, two accelerometers, two rate gyroscopes, a minimum of one brake line pressure sensor, and a steering wheel angle sensor. A processor capable of five million floating-point operations per second is required to implement the numerical techniques. This is requirement is satisfied by current personal computer technology. The project findings clearly demonstrate the ability of the numerical techniques developed to provide information necessary for ITS and AVCS product development.

IDEA PRODUCT

Intelligent Transportation Systems (ITS) require dynamic information concerning safe vehicle operation during every driving situation; a system must know whether a vehicle is capable of performing a required maneuver before making driving decisions. This project provides quantitative techniques for determining information necessary to make and implement intelligent driving decisions. The results have application to the following:

1) Developing ITS products for automated driving, emergency intervention, and driver safety aids; and

2) Implementing AVCS to improve vehicle stability and drivability.

Processing algorithms developed in this project determine road coefficient of friction. Road friction can be used to estimate other parameters, such as stopping distance, brake power required to stop, and vehicle maneuverability, required to make driving decisions. In addition, the algorithms provide feedback signals that can be used to design AVCS that increase vehicle stability and handling qualities.

CONCEPT AND INNOVATION

The numerical procedures developed in this project are based on extended Kalman filtering, a nonlinear adaptive filtering method (1). Similar methods have been used successfully in analogous problems concerning modeling of aircraft dynamics (2,3). The adaptive filter requires a dynamic model of the vehicle and data that is gathered continually from sensors on board the vehicle. Ground vehicle motion depends largely on the tire forces, or forces that cause deceleration and traction and that can prevent a vehicle from losing lateral stability or "spinning" during severe maneuvers. The tire forces are nonlinear, and they depend on uncontrollable factors, such as tire/road-surface coefficient of friction (u), tire pressure and wear, and vehicle loads. While the latter parameters can be measured using standard sensors, there is currently no way to measure or otherwise determine u. In this project, the tire forces and motion are determined using extended Kalman filtering and measurements from standard off-the-shelf sensors. The forces and motion serve as inputs to a Bayesian Hypothesis Selection procedure that compares the estimated forces and motion to outputs of a tire force model to determine the correct u from a set of hypothesized values. Road coefficient of friction is extremely important to predicting stopping distances, safe following distances, and maneuverability; given an estimate of CL, information required to make on-the-spot driving decisions can be determined.

This project is unique in its focus on providing high-quality information for decision-making and feedback control using transducers and computer technology that are currently available. While research by other investigators has considered ITS decision-making methods (43, there is little current research on providing the information required to make intelligent driving decisions. Such information depends on many factors, changes continually, and must be continually updated. A "road friction transducer", while useful for many ITS products, would be difficult to design at best. The methods developed in this project provide the necessary road friction estimate without requiring a road friction transducer and at the same time supply signals required for AVCS. Prior AVCS research has shown that feedback signals such as wheel slip, wheel slip angle, and vehicle velocity give performance gains over control systems currently used in some vehicles (6,7,8); however, these signals also cannot be measured using current sensor technology mounted on-board the vehicle. The EKF also provides such signals making it possible to commercially implement vehicle control systems that increase safety and maneuverability

INVESTIGATION

Two project stages were conducted as part of this investigation. The objective of Stage 1 was to develop and validate adaptive filtering algorithms using computer simulation. An eight degree-of-freedom model of a 1990 Ford Taurus (9) and an analytic tire force model (10) were used to simulate true vehicle motion from which noisy sensor measurement histories were constructed. The measurement histories served as inputs to the estimation algorithm. A variety of steering and braking maneuvers ranging from modest to severe were simulated to determine EKF and road friction estimation performance over a broad range of driver inputs, A study was conducted for open-loop operation of a braking system that incorporates the algorithms to assess robustness to reasonably expected uncertainties in the system model. Examples of parameters required for ITS decision making were determined along with typical parameter uncertainties. Potential benefits of the algorithms developed to advanced feedback control were assessed by quantifying performance gains in simulated braking control systems that incorporate the algorithms developed.

Stage 2 of the project involved a final verification task using recent field test data for a 1994 Ford Taurus from the National Highway Traffic Safety Administration's Vehicle Research and Testing Center (VRTC) in East Liberty, Ohio. For this task, the computer model of the vehicle was replaced with actual field test data and the algorithms were verified to the extent possible using that data. This stage provided a low cost method of verification using existing data before

launching an applied testing and full-scale evaluation project. The final product of the second stage included expanded verification of the algorithms developed in Stage 1 and readiness to initiate real-time implementation and evaluation. Implementation requirements were assessed based on transducers assumed for simulation, transducers used to collect field test data, and computation requirements.

All simulation and field test data processing was performed using MATLAB v4.1 *(11)*. Appendix A gives the vehicle equations of motion used for simulation and extended Kalman filter implementation equations. Table 1 provides vehicle parameters for the simulated vehicle and test vehicle. Figure 5 defines the sign conventions and parameters for the eight degree-of-freedom vehicle model. The remainder of this section details the investigation and results of each project stage.

TABLE 1 Vehicle simulation model and field test vehicle parameters

Parameter	Simulation model	Field test vehicle
Distance: cg to front and rear axle, L_f, L_r	1.2, 1.5 m	0.92, 1.77 m
Distance: sprung mass cg to vehicle cg, e	0.198 m	-0.033 m
Distance: roll axis to sprung mass cg, h	0.183 m	0.47 m
Front & rear track width, t_f, t_r	1.56, 1.54 m	1.56 1.53 m
Wheel radius, R_W (=h_{uf}, h_{ur})	0.32 m	0.31 m
Front & rear roll center height, h_f, h_r	0.277, 0.017 m	0.13, 0.11 m
Sprung mass, m_s	1702 kg	1290 kg
Front and rear unsprung mass, m_{uf}, m_{ur}	81.2, 91.6 kg	98.1, 79.5 kg
Moment of inertia about yaw axis, I_{zz}	2526 kg-m^2	2798 kg-m^2
Moment of inertia about roll & yaw axes, I_{xz}	61.7 kg-m^2	0 kg-m^2
Wheel moment of inertia, I_W	1.07 kg-m^2	0.99 kg-m^2
Sprung mass moment of inertia about roll axis, I_{xxs}	489 kg-m^2	683 kg-m^2

Development of Adaptive Filtering Algorithms

Estimation of vehicle motion and tire forces that serve as inputs to the road friction identification block of Figure 1 is performed using an Extended Kalman Filter (EKF) *(1)*. The purpose of the EKF is to estimate vehicle motion, or state from an incomplete, noise corrupted measurement set. The vehicle state vector ($\mathbf{x}(t)$) components are vehicle longitudinal and lateral velocity (v_x and v_y), four wheel angular velocities (ω_{fl}, ω_{fr}, ω_{rl}, ω_{rr}), yaw rate (r), roll rate (p), and roll angle (ϕ). The vehicle estimation model used by the EKF includes the equations of motion of the vehicle given in App. A, but requires no tire force model or knowledge of road coefficient of friction. Instead, tire forces are treated as unknown parameters, and the state vector $\mathbf{x}(t)$ is augmented to include differential equations for each force to be estimated *(12)*. Careful study of the equations of motion shows that the longitudinal tire forces at each wheel (F_{xfl}, F_{xfr}, F_{xrl}, F_{xrr}) and front and rear per axle lateral tire forces (F_{yf}, F_{yr}) can be determined using a sensor set that does not require direct measurement of tire forces. A second-order random walk model is appended to the vehicle equations of motion to model each unknown force:

$$\begin{bmatrix}\dot{y}_0\\ \dot{y}_1\end{bmatrix}=\begin{bmatrix}0 & 1\\ 0 & 0\end{bmatrix}\begin{bmatrix}y_0\\ y_1\end{bmatrix}+\mathbf{w}_y \tag{1}$$

y_0 represents the force to be estimated, y_1 is its first time derivative, and $\mathbf{w}_y$ is random, white noise. Appending second-order random walk models for tire force to be estimated results in a 21st-order estimation model. Denoting estimated variables as ($\hat{\cdot}$) and the nonlinear vehicle equations of motion as $\mathbf{f}(\mathbf{x}(t),\mathbf{F}(t),\mathbf{u}(t))$, the augmented nonlinear differential equation that models the vehicle in the estimator is

$$\dot{\hat{\mathbf{x}}}_A(t)=\begin{bmatrix}\dot{\hat{\mathbf{x}}}(t)\\ \dot{\hat{\mathbf{F}}}(t)\end{bmatrix}=\begin{bmatrix}\mathbf{f}(\hat{\mathbf{x}}(t),\hat{\mathbf{F}}(t),\mathbf{u}(t))\\ \mathbf{A}\,\hat{\mathbf{F}}(t)\end{bmatrix}=\mathbf{f}_A(\hat{\mathbf{x}}_A(t),\mathbf{u}(t)) \tag{2}$$

$$\hat{\mathbf{y}}(t)=\mathbf{h}_A(\hat{\mathbf{x}}_A(t),\mathbf{u}(t)) \tag{3}$$

where $\mathbf{A}$ is a block-diagonal matrix, $\hat{\mathbf{x}}_A(t)$ is the augmented state vector, and $\hat{\mathbf{y}}(t)$ is the output reconstructed based on the estimation model and the state estimate. A discrete-time extended Kalman filter is implemented by integrating eq. 2 and a continuous-time matrix Riccati equation to propagate the state and error covariance estimates, computing the filter gain matrix, and updating the state and covariance estimates based on the measurement residual *(1,12)*. Slip,

slip angle, and velocity estimates ($\hat{s}$, $\hat{\alpha}$, $\hat{v}$) at each wheel are derived kinematically from the state estimate. Details concerning EKF implementation are given in Appendix A.

Determining Road Coefficient of Friction

A nominal tire force model can be constructed by using analytic modeling techniques *(10)* or by regressing EKF force vs slip data at fixed normal force and road surface *(12)*. Such a model provides longitudinal and lateral tire forces as functions of slip, slip angles, normal force, μ, and wheel velocities. With a nominal tire force model available, μ can be estimated recursively by statistically comparing the forces estimated by the EKF to those that result from the tire force model for a particular μ. Figure 6 represents this procedure. Given a tire model and its inputs, the outputs, longitudinal and per axle lateral forces, are nondimensionalized by their respective normal forces ($\mathbf{F_Z} = [F_{Zfl}\ F_{Zfr}\ F_{Zrl}\ F_{Zrr}]$) to define the normalized tire force vector $\boldsymbol{F}$:

$$\boldsymbol{F} = [F_{xnfl}\ F_{xnfr}\ F_{xnrl}\ F_{xnrr}\ F_{ynf}\ F_{ynr}] = \boldsymbol{T}(s,\alpha,\mathbf{F_Z},v,\mu) \tag{4}$$

The function $\boldsymbol{T}$ in eq. 4 represents the nonlinear tire force model. Denoting $\hat{\boldsymbol{F}}$ as the EKF estimate of the true tire force vector, the conditional probability density function of $\hat{\boldsymbol{F}}$ given μ is

$$\mathrm{pr}[\hat{\boldsymbol{F}} \mid \mu] = \mathrm{pr}[\hat{\boldsymbol{F}} \mid \boldsymbol{T}(\hat{s}, \hat{\alpha}, \hat{\mathbf{F}}_Z, \hat{v}, \mu)] = \frac{1}{(2\pi)^{n/2}\mathbf{P}^{1/2}} e^{-1/2\,(\hat{\boldsymbol{F}} - \boldsymbol{T})^T \mathbf{P}^{-1}\,(\hat{\boldsymbol{F}} - \boldsymbol{T})} \tag{5}$$

Equation 5 expresses the probability density of obtaining the forces $\hat{\boldsymbol{F}}$ given a particular value of μ. $\mathbf{P}$ is an n x n covariance matrix, and n is the size of vector $\boldsymbol{F}$. The EKF estimates of slip, slip angle, and wheel velocity, along with estimates of the normal force at each wheel serve as inputs to the tire force model given an hypothesized μ to compute the probability in eq. 5. Given J hypothesized values of μ, the most likely value is computed at each sample time using Baye's rule *(1)*. At time t_k, the conditional probability of hypothesis μ_j given $\hat{\boldsymbol{F}}_k$ is

$$\Pr[\mu_j \mid \hat{\boldsymbol{F}}_k] = \frac{\mathrm{pr}[\hat{\boldsymbol{F}}_k \mid \mu_j]\ \Pr[\mu_j \mid \hat{\boldsymbol{F}}_{k-1}]}{\sum_{j=1}^{J} \mathrm{pr}[\hat{\boldsymbol{F}}_k \mid \mu_j]\ \Pr[\mu_j \mid \hat{\boldsymbol{F}}_{k-1}]} \tag{6}$$

The most likely value of μ from among the hypothesized values is then given by a weighted sum:

$$\hat{\mu}_k = \sum_{j=1}^{J} \Pr[\mu_j \mid \hat{\boldsymbol{F}}_k]\ \mu_j \tag{7}$$

$\hat{\mu}_k$ represents the estimated value of road friction. The algorithm starts by specifying the set of hypothesized values and the initial conditional probabilities $\Pr[\mu_j \mid \hat{\boldsymbol{F}}_o]$. If no a-priori knowledge of road friction is available, each hypothesized value is given an initial equal conditional probability of being true. The most likely value is determined by updating the probabilities at each sample time using eq. 5-7. Since the hypothesis vector includes discrete values of the continuous variable μ, the true value of road friction may not match an hypothesis. In this case, the conditional probabilities of two hypotheses around the actual value of μ may contribute to the weighted sum in eq. 7, or, the conditional probability of a single hypothesis closest to the underlying value may converge to 1, while other conditional probabilities approach zero. In this case, the worst-case error for the μ estimate is less than $\pm\Delta\mu$, where $\Delta\mu$ is the increment between hypothesis values.

Using the method above, μ estimation is separate from the EKF, and μ estimation results do not affect state estimates directly. The EKF provides state estimates for feedback control and for determining μ. Once μ is estimated, information such as peak slip, minimum stopping distance, and lateral maneuverability can be determined for ITS decisions. However, because the two tasks are separate, state estimates can be used for feedback before the μ estimate converges. This scenario is vital for good stability and robustness properties.

Stage 1 Simulation Results

Evaluation of the Extended Kalman Filter

Pure steering, pure braking, and combined steering and braking maneuvers of varying severity were simulated for evaluation of the EKF in Stage 1. Tracking ability during emergency situations was determined by simulating an open-loop panic maneuver on a road with several sudden changes in μ. Figure 2 shows the results; here, the braking input is T_b = 3000 N-m, and the front axle steering input is δf_o = 0.15 rad, corresponding roughly to a 135 degree handwheel

angle. The road friction coefficient is $\mu = 0.3$, $0 \# t < 0.5$ sec, $\mu = 0.85$, $0.5 \# t < 1.5$ sec, $\mu = 0.3$, $1.5 \# t < 2.25$ sec, and $\mu = 0.5$, $2.25 \# t < 3.0$ sec. The EKF slip, zip angle, and force estimates (dashed lines) approximate the actual trajectories (solid lines) well, even in the face of abrupt changes in μ and severely nonlinear tire forces. The steering and braking inputs in Figure 2 are severe, particularly for the low friction road surface, causing all four wheels to lock. Because it is important to know vehicle parameters before an emergency situation ensues, it is important for the EKF to perform well during normal driving as a vehicle performs routine stops and turns. Figure 7 shows example EKF results for less severe braking (0.25g longitudinal deceleration) and steering (0.45g peak lateral acceleration) on a $\mu = 0.825$ road surface. The inputs correspond roughly to a turn and stop maneuver from highway speed, as in exiting a freeway onto an off ramp. Tracking of the actual forces by the EKF shown in Figures 7a and 7b is excellent. The results presented in Figures 2 and 7 represent two extremes of maneuvering considered for evaluation of the EKF; inputs between these extremes were considered as well, with excellent estimation results . Force, slip, and slip angle trajectories provided by the EKF are used below to determine μ.

Evaluation of road coefficient of friction estimation

The road coefficient (μ) identification procedure requires a covariance matrix, P, hypothesis set, and initial estimates of conditional probabilities, $Pr[\mu j \,|Fk\,]$. Diagonal components of P serve as weighting factors, enabling the user emphasize particular components of the tire force vector in the selection algorithm. For instance, during pure braking, P = diag([0.0l 0.01 0.01 0.01 1.25 1.25]) places equal emphasis on each on the longitudinal forces and less emphasis on the per-axle lateral forces. For pure steering maneuvers, P is selected to place more emphasis on lateral forces. The hypothesis set is μ = [0.25 to 0.85] in 0.05 increments. Computation burden per hypothesis is small, and a hypothesis set with small increments produced good results. Equal probability of each hypothesis being true was selected at t = 0, i.e., there is no a prior knowledge of μ. The conditional probabilities where not allowed to drop below $\varepsilon = 0.00001$, enabling the algorithm to respond quickly to sudden changes in μ.

Figure 8 shows the road coefficient of friction estimate, normal forces, and $Pr[\mu j \,|Fk\,]$ histories for the trajectory of Fig. 2. Tracking of the actual road coefficient of friction is excellent. The condition probability ($Pr[\mu j \,|Fk\,]$) histories show that the algorithm quickly converges to two hypotheses around the actual p, while the remaining probabilities become small. The algorithm responds instantly when u changes suddenly. Figure 7c shows identification results for the more modest turn and stop maneuver. While convergence of the road friction estimate is slow, compared to the severe maneuvering case, the algorithm does converge to within one hypothesis of the actual road friction, $\mu = 0.825$. The actual road friction here is modeled as a random constant whose mean value is 0.825, and the mean value does not correspond to one of the hypothesized values. Primary importance for μ estimation during modest maneuvering is not the settling time of convergence, but that the μ estimate represents actual road friction.

Figure 7 reveals limiting behavior of the road friction identification algorithm. While EKF performance is excellent for all maneuvers considered, road friction identification ranges from very difficult, for extremely “small” inputs to very easy for “large” inputs. The behavior can be explained in the context of Figure 9, which shows normalized longitudinal and lateral forces as a function of μ based on an analytic tire force model (*10*). At low slip ratios and slip angles typical of small input maneuvers, it is difficult to distinguish between curves of fixed μ, since the force-slip relationship is linear and is nearly independent of μ. Hence, the μ identification algorithm performs very well above slip ratios of approximately 0.05 and has some trouble distinguishing between hypotheses for smaller slip ratios. Similar behavior is apparent for pure steering inputs that generate slip angles less than approximately 0.1 rad (Figure 9b). To further assess the μ identification algorithm, a variety of steering and braking inputs were considered on a variety of simulated road surfaces. Figure 10 shows example results. In Fig. 10a-d, actual values of μ match one of the hypothesized values and in Fig. 10e-f actual values of μ do not match one of the hypothesized values. In Fig. 10a-d, the estimated μ converges to the actual value in all except one case, and the worst case 5% settling time is 0.73 sec. In Fig. 10e-f, μ settles to a hypothesized value just greater than or just less than the actual value; hence, the estimated μ is always within 9.05 (one hypothesis) of the actual μ. The single case that does not converge can be explained in the context of the tire force curves, as the corresponding slip ratios are small (below 0.04). At slightly higher slip ratios that are still below that corresponding to peak longitudinal force, the algorithm performs well. μ identification for the pure steering maneuver exhibits a high settling time largely because the corresponding slip angle response is slow; Figure 9b shows that for small slip angles, it is also difficult to distinguish between μ hypotheses.

Modeling Requirements and Robustness

The μ identification procedure requires a vehicle model (for the EKF) and tire force model. The tire force model is likely to be uncertain, as it depends on experimental and/or analytic modeling, and it can change over time with uncertain tire pressure and wear. Some vehicle model parameters are also likely to be uncertain, as vehicle load (mass)

depend on the number of passengers, fuel mass, and cargo mass. Uncertainties in vehicle load affect the center-of-gravity location, sprung mass, and moment of inertia parameters given in Table 1. In the results presented above, the tire force model used in the μ identification procedure was identical to the tire force model used to simulate vehicle motion, and the vehicle parameters assumed in the simulation model matched the estimation model. A simple robustness study was conducted by mismatching the simulation and estimation tire models and vehicle load. Significant mismatch in the tire model was introduced by selecting a tire for the μ identification procedure that did not match that of the actual vehicle. In addition, worst-case vehicle load uncertainty was introduced; the vehicle load assumed in the simulation corresponds to driver-only conditions, and the estimation model assumed a fully loaded vehicle. Figure 11 shows the EKF results for the trajectory of Figure 2 when these uncertainties are introduced. Load uncertainties are reflected in the mismatch between estimated (dashed) and actual (solid) signals. The longitudinal force trajectories follow actual forces extremely well, while lateral force estimates show a modest bias. All other estimated variables remain largely unaffected by the parameter uncertainties considered.

Load uncertainty has the potential to cause significant performance robustness problems in road friction identification because the procedure depends heavily on knowledge of the normal forces to normalize longitudinal and lateral tire forces. A solution to these concerns is to include a static load sensor in the transducer set to measure the static sprung mass load ($m_s g$). μ identification results in the face of tire model and load uncertainties are presented in Figure 12. Two cases are considered in Figure 12. The dotted line shows the μ estimate for load and tire model uncertainties, where the normal force estimate is based on the uncertain load (i.e., assuming no static load transducer). The dashed line gives the μ estimate when the normal force is based on a transducer measurement of static load, while other load parameters (center-of-gravity location, sprung mass, and moment of inertia) remain uncertain. Sensitivity of the procedure to normal force uncertainties is significant at high values of μ, causing up to 0.15 error in the μ estimate (dotted line). For errors in other load parameters and tire model error the μ estimate converges to within one hypothesis of the actual value (dashed line).

AVCS Performance Benefits

State estimates from extended Kalman filtering provide feedback signals that can be used to design vehicle control systems that are substantially different from current technology. Possible control systems include slip control tractive and braking systems, tire force feedback systems, and full state feedback systems. In this study, performance benefits of such systems over existing vehicle control system technology are considered. The emphasis of this task is not on control system design, but on demonstrating possible performance gains if the EKF and μ identification algorithms were available to a controller. Typical control benefits are assessed by comparing the performance of four braking systems: 1) no anti-lock braking system (ABS) (open-loop braking system); 2) a vehicle with ABS that cycles between two slip values (ABS); 3) a vehicle with slip-control braking, assuming feedback of perfect wheel slip signals and no disturbance inputs (PRYideal); and 4) a vehicle with slip-control braking, assuming an EKF provides slip estimates for feedback (PID/EKF). The first system represents that available on the majority of current vehicles. The second system is an idealization of ABS systems available as optional equipment on some vehicles; because ABS operation is proprietary information, this system does not necessarily model a particular ABS, but approximates typical ABS operation of cycling the brakes to avoid wheel lock. The ABS system modeled here is idealized because perfect wheel slip signals are assumed to be available to determine incipient wheel lock. Real ABS systems normally base this determination on wheel angular velocity. The third system represents the “ideal”, or best possible performance for a given “slip control” braking system (SCBS), or system that seeks to control wheel slip to a certain value. System 3 cannot be implemented, since slip cannot be measured directly. The last system represents achievable performance using a stochastic slip control braking system modeled in Figure 1. Here, slip setpoints for the PID/EKF system are generated based on a μ estimate and nominal tire model, and a simple PID controller (12) maintains the setpoint. For straight-line braking, the setpoint corresponds to the peak slip value, or slip corresponding to maximum longitudinal force. Figure 13 shows an example of actual and estimated peak slip setpoints for a controlled braking maneuver on a $\mu = 0.5$ road surface, and straight line stopping distances from 55 mph for $\mu = 0.3$ and $\mu = 0.85$ are shown in Fig. 14. The peak slip estimates approximate actual peak slip very well until the last 0.5 set of the trajectory, where velocity approaches zero and signal-to-noise ratio in the slip estimate increases. Figure 14 shows that feedback of a slip estimate introduces no noticeable performance degradation over an ideal SCBS. The PID/EKF stopping distances are 11% to 25% lower than those of systems with no ABS, and 5.5 to 6.5% lower than the simulated ABS system, representing significant potential gains. Since the simulated ABS system is based on cycling between two slip values and assumes slip is known without error, actual ABS may not perform as well as the ABS simulated here, and performance gains of slip control systems may be higher.

Degrees of lateral maneuverability can be achieved in a SCBS by adjusting the slip setpoint; operating at the “peak slip” maximizes longitudinal force at the expense of lateral force, while operating below the peak slip increases lateral

force. Current ABS systems that cycle around peak slip can lose lateral stability in some situations. Figure 15 compares the four braking control systems for a combined steering and braking maneuver on a $\mu = 0.85$ road surface. The slip setpoints for the PD controllers are adjusted to give similar maneuverability as the simulated ABS system. With no control, the wheels lock, and lateral forces are extremely small. The ABS system loses stability for the emergency maneuver considered. The PID systems are able to sustain the same lateral maneuverability as the ABS system with no loss of stability, achieving peak longitudinal and lateral accelerations of approximately 0.6g. There is little difference between the paths of the ideal and PID/EKF vehicles, indicating no loss in performance due to slip setpoint estimation and slip estimate feedback. These results show possibilities for significant improvement in vehicle lateral stability using AVCS that incorporate the numerical procedures developed.

A nominal ABS that cycles between two slip values is limited adjustability of lateral maneuverability. Achievable ranges of lateral maneuverability are given in Fig, 16 for the PID/Ideal and PIINEKF systems and two different road conditions. The tradeoff between longitudinal and lateral acceleration is determined by adjusting the slip setpoint as some percent of the peak slip value estimated. Operating at "100 % peak slip" corresponds to maintaining a value of slip that maximizes longitudinal force. At less than 100% peak slip, the slip setpoint is below the value that maximizes longitudinal force, reducing available stopping force and increasing lateral forces. For each road surface, variations in longitudinal and lateral accelerations are indicated by the small differences between the paths of the stochastic braking control system and the ideal system. These plots demonstrate how well the vehicle can follow an intended path using an AVCS.

Decision Parameter Determination

Figure 13 gives an example of the type of information that can be derived knowing μ. Here, the value of slip corresponding to peak longitudinal force, or "peak slip" is derived from a look up table given the EKF slip and slip angle estimates, the static normal forces, and the μ estimate. The peak slip value can be used as a control setpoint for traction control , braking control , or stability augmentation. Other parameters can be derived from the μ estimate that play an important role in ITS decision-making. This section gives examples of such parameters and their uncertainties.

Point-mass kinematics provides a simple means of estimating minimum stopping distance or safe velocity as a function of μ and vehicle load; for a given braking control system, road coefficient of friction corresponds to a maximum achievable deceleration, from which stopping distance from current velocity is predicted. When μ is known perfectly, the maximum error in predicted stopping distance from highway speeds based on this method is 0.93 m, over a range of μ from 0.3 to 0.85; maximum error occurs at t = 0, and it was determined by simulating controlled braking maneuvers assuming perfect feedback of slip signals. When μ is estimated, the error in minimum stopping distance estimate depends on the error in the p estimate. Figure 17 shows the minimum stopping distance estimate (solid line) as a function of road friction for velocities from 10 m/s to 25 m/s. The dashed lines represent uncertainties in the stopping distance estimate for uncertainty in p estimate of _+.05 (one hypothesis). Another important parameter that can be assessed based on the μ estimate is the brake ratio, or measure of brake power required for a rear vehicle to avoid an accident with a front vehicle (*4*). Assuming a target velocity, v, and an initial velocity v_o, for the rear vehicle, the brake ratio can be defined as

$$br = \frac{v^2 - v_0^2}{2d\Delta x} \tag{8}$$

where d is the maximum achievable deceleration and Δx is the separation distance between vehicles. d is linearly related to μ. Figure 17b gives an example of brake ratio and uncertainty bands based on _+.05 error in the μ estimate for a vehicle traveling at 55 mph approaching a vehicle traveling at 30 mph, for two separation distances. An ITS can use information such as that presented in Fig 17b to determine the probability of safely performing a braking maneuver or the safe vehicle velocity required to minimize the probability of an accident. For example, on a low friction road ($\mu = 0.3$), the brake ratio for $\Delta x = 75$ m is between 0.77 and 1.05, indicating that there is a possibility of exceeding the total available braking power if a straight line braking maneuver is performed. For the larger separation distance, just over half of the available braking power (between 0.46 and 0.63) is required to achieve the target velocity. Uncertainty intervals decrease with increasing road friction, as indicated in the figure.

Stage 2 Results

Field test data were provided by VRTC for Stage 2 evaluation (13). All maneuvers were open-loop, fixed-input runs conducted by VRTC as part of their standard vehicle testing and modeling procedures. A single straight-line braking maneuver was provided from a late 1994 test data set, and straight line braking maneuvers ranging from 2 m/s^2 to the maximum deceleration possible for the test vehicle (approx. 8.5 m/s^2) were provided based on recent (August 1995) field testing. Pure steering data provided by VRTC included ramped steering maneuver data and J-turn (constant steer

input) data. Severe combined braking and steering data also were provided. All data were collected from maneuvers on dry asphalt; no data were available for wet pavement.

Since the simulation model is replaced by actual field test data for Stage 2 evaluation, time histories of actual vehicle state and road friction do not exist for evaluating the EKF and μ estimate results. In the absence of actual signals with which to compare estimated signals, the Stage 2 results must be judged based on consistency of the road friction estimate to that expected for dry asphalt and for consistency with simulation results. For a sample of field test cases, a simulation was conducted for identical inputs, assuming a true underlying road friction coefficient approximately equal to that identified by processing field test data. The resulting simulated motion was compared to field test data results. The hypothesis set for field test data processing was p = [0.25 to 0.9] in 0.05 increments, as processing results indicated the possibility of friction coefficients greater than 0.85 for field test data. The field test vehicle parameters are given in Table 1.

Pure braking results

Figure 4 shows the EKF tire force estimates and road friction estimates for a straight line braking maneuver from highway speeds on dry asphalt[2]. The average and peak decelerations for this maneuver are 0.35g and 0.4g, respectively, and road friction converges to 0.90. This maneuver is typical of normal braking from highway speeds in which the wheel slip vs longitudinal force relationship remains in the linear region of the tire force curves (Fig. 9a). In the absence of lateral inputs, lateral forces (not shown) are small. While the underlying road friction and tire forces for this maneuver are unknown, results can be judged by simulating an identical maneuver on a high friction road surface and comparing forces estimated from field test data to simulated forces. The dashed trajectories in Figure 4 provide simulation results for identical inputs and a true underlying road friction of 0.88. The mean values of the simulated and estimated longitudinal forces are nearly indistinguishable, indicating excellent EKF results. Table 2 summarizes the ERR force estimate results for this run. Column 3 of Table 2 gives the correlation coefficient between simulated tire forces histories and EKF force estimates from field test data processing. Road friction estimates for simulated and field test data are 0.88 and 0.9, respectively. Measurement of road friction at similar test facilities on dry asphalt indicate typical road friction values for dry asphalt of 0.85 to 1.0 (*14*). Figure 18 shows results of processing straight line braking field test data for decelerations of 2 m/s^2, 3 m/s^2, 5 m/s^2, 7.5 m/s^2, and maximum deceleration achievable with the test vehicle's ARS system active. In each case, processing of field test data begins when the brakes are applied. The transient response of the braking system is indicated by the time it takes for the forces to reach a steady-state value. The steady-state value of longitudinal tire force estimates increases with deceleration, as expected. With the exception of Figure 18e, slip ratios at each wheel (not shown) remain approximately constant. In Figure 18e, with the ARS system active, the brakes begin to cycle on and off when the system detects incipient wheel lock, as reflected in the force response. Road friction identification results are consistent with what is expected for dry asphalt, with the exception of the 2 m/s^2 (0.29) braking maneuver. Here, the tire forces are simply too small to distinguish road friction; this is consistent with Stage 1 simulation findings, which indicated limitations to road friction identification for small tire force inputs. As the braking input and resulting forces increase, the speed of the transient road friction response improves.

TABLE 2 Comparison of simulation and field test data results for 0.35g braking

Variable	Mean Value, simulation	Mean value, field test data estimate	Correlation coefficient
Front left long, Force, Fxfl	1570 N	1572 N	0.99
Front right long, Force, Fxfr	1606 N	1609 N	0.99
Rear left long, Force, Fxrl	1306 N	1309 N	0.96
Rear right long, Force, Fxrr	898 N	903 N	0.98

Pure steering results

Figure 19 shows estimated lateral forces and road friction from field test data for a slowly increasing steering input at a vehicle velocity of a proximately 17.5 m/s (39.1 mph) along with simulated forces and simulated road friction estimate for the same inputs[2]. This maneuver was also conducted on dry asphalt. The simulated data assumed an underlying road friction of μ = 0.88. The steering input for this maneuver is ramped to 1.36 rad (78 degrees) over the duration of the test run. The correlation coefficients between simulated and estimated lateral tire forces are 0.98 and 0.92 respectively, for the front and rear axles indicating good EKF performance. In both simulation and field test data results, the road friction estimate convergence is slow because of the slow slip angle and lateral force response,

revealing small steering input limitations to road friction estimation. The lateral acceleration reaches -0.4g at the time road friction converges to 0.9. Figure 20 shows estimated road friction for more recent (June 1995) slowly increasing steering input field test data at three velocities: 12 m/s (27 mph), 22 m/s (49 mph), and 32 m/s (72 mph). The steady-state road friction estimates are 0.83,0.89, and 0.90. Figure 19 also shows estimated lateral forces and road friction for a 0.4g J-turn (constant steering input) at 11.2 m/s (25 mph). Again, agreement with road friction expected for dry asphalt is good for all pure steering cases considered.

Combined braking and steering results

Figure 2 1 shows the EKF and road friction estimation results for hard braking and steering field test data near the limits of vehicle capabilities (peak a_x = 0.9g and peak a_y = 0.8g). For the maneuver considered, the vehicle's antilock braking system is enacted, as indicated by the oscillatory brake line pressure measurements and resulting tire force estimates. For the EKF simulation road friction was assumed to be 0.88. Correlation coefficients for the forces simulated and those estimated from field test data given in Table 3 show excellent agreement between the simulation and field test data for three of four longitudinal forces. For the simulated run (dashed lines) the front left wheel locks, and the corresponding longitudinal tire force saturates. The lateral forces generated for field test data are greater in magnitude than simulated lateral forces. Force and slip comparisons of simulated and field test results for identical inputs indicate that either the actual road friction is higher than that assumed for simulation, or the tire force model used in road friction identification is not accurate in predicting tire forces near the limit of vehicle performance. (The peak accelerations for the simulation were a_x = 0.8g and peak a_y = 0.6g.) Nevertheless, results of processing this test run indicate good EKF performance and road friction identification results for severely nonlinear tire forces and significant transients in the braking inputs.

TABLE 3 Comparison of simulation and field test data results for severe braking and turning

Variable	Correlation coefficient
Front left long, Force, Fxfl	0.31
Front right long, Force, Fxfr	0.98
Rear left long, Force, Fxrl	0.91
Rear right long, Force, Fxrr	0.95
Front per-axle lat force, Fyf	0.88
Rear per-axle lat force, Fyr	0.73

Computation, Sensing, and Modeling Requirements

The EKF requires 131K floating point operations (FLOPS) per sample time to propagate the state estimate (8 nonlinear and 13 linear equations) and a 21 x 21 state covariance matrix using fourth-order Runge Kutta integration. The μ identification algorithm requires 600 FLOPS per sample time per hypothesis, including calls to the analytic tire force model to evaluate eq. 6. For 13 hypotheses, a total of approximately 139K FLOPS per sample time are required to implement the EKF and μ identification procedure. Sample times of 0.025 and 0.03 set were used to generate the simulation results in this paper, and sample times up to 0.1 seconds did not cause integration instability or unacceptable degradation in the state estimates or u identification results. For such sample times and computation speeds, a 1.4 to 5.6 MFLOP processor is required; Power-PC and Pentium-based personal computers are capable of such computation speeds. The computation burden was determined without attempting to introduce efficient algorithms in the EKF. The EKF requires numerical integration of a symmetric covariance matrix (1); since the covariance matrix is symmetric, the covariance propagation can be modified to incorporate computation reducing algorithms and computation burden can be reduced.

All instrumentation (transducers and computing equipment) required to implement the numerical procedures in real-time is off-the-shelf equipment. The instrumentation set assumed for simulation includes four tachometers, two rate gyroscopes, two linear accelerometers, a position encoder, and a brake line pressure transducer. The field test data instrumentation set included a brake line pressure sensor for each wheel in addition to the other sensors. A static load transducer can be included to improve performance as vehicle loads change. The measurement noise associated with the transducers assumed for the simulation is given in Table 4 along with the variance measured from raw field test data. With the exception of the wheel tachometers, the transducers assumed in simulation results were of similar quality to those used by VRTC to collect field test data, The wheel tachometers assumed for simulation were of lower quality.

TABLE 4 Measurement noise variance for transducers

Signal	Variance used in simulation	Variance measured [6]
Accelerations, (a_x and a_y)	0.05 $(m/s^2)^2$	0.018 to 0.08 $(m/s^2)^2$
Wheel angular velocities	0.1 $(rad/s)^2$	0.0012 to 0.0029 $(rad/s)^2$
Angular rates (r and p)	0.0001 $(rad/s)^2$	0.000012 to 0.00023 $(rad/s)^2$

In addition to the required instrumentation, a vehicle model, along with parameters given in Table 1 must be available. The four-wheel (eight degree-of-freedom) vehicle model used in the EKF proved to be adequate for estimating tire forces, and it is not difficult to determine parameters for such a model. While the eight degree-of-freedom model provides wheel slip estimates at each wheel that can be used for AVCS, it is possible to perform the road friction estimation procedure using a lower-order vehicle model, such as the five degree-of-freedom "bicycle" model of (6). This would reduce processor computation requirements. An analytic tire model is required for road friction identification, and parameters for the vehicle's tires are required for this model. The tire parameters for the field test vehicle in this study were provided by VRTC based on their own in-house tire testing. The robustness study showed a small degradation in road friction estimate (_+0.05 error) when tire model contained error; however, the robustness study considered only mismatch based on two different sets of tire parameters. Since tires differ significantly from vehicle to vehicle, and even similar tires manufactured by different companies can differ, tire parameters must be available for every manufactured tire on the market in order to implement a road friction identification procedure that can detect small changes in road friction. Nevertheless, it is also possible to implement the road friction identification algorithm as a qualitative driver safety aid simply by requiring the procedure to distinguish between "low", "medium", and "high" road friction coefficients. In this case, the hypothesis set may contain only three possible values of road friction to distinguish between, a lower-order vehicle model can be used, and the algorithm will be more robust to vehicle and tire parameter uncertainties.

PLANS FOR IMPLEMENTATION

In an effort to promote visibility of the numerical procedures developed in this project, results of Stage 1 of the IDEA project have been published in two conference proceedings (*15,16*), and results of Stage 2 will be reported in a Society of Automotive Engineers paper (*17*). One or more comprehensive papers will be prepared for journal publication. Road friction estimation has immediate application to the development of driver safety aids or warning devices in which control of a vehicle is not removed from the driver (*18*). In addition, results are of interest to tire manufacturers and research groups seeking to understand and model tire force and vehicle dynamics interactions. This final report will be made available to all parties who have expressed interest in receiving it in order to develop at least one partnership with a research group or company that expresses interest in further evaluation and/full scale implementation an ITS product or AVCS based on this study.

Before proceeding with full scale testing it is recommended that evaluation of the EKF and road friction identification procedures performed using field test data be extended to include processing of field data from different road surfaces. In addition, field test data from "normal" driving involving stopping, turning comers, and following road curvature should be considered in addition to open-loop fixed steering/braking inputs provided by VRTC.

CONCLUSIONS

This feasibility study provides numerical techniques that can be used in ITS products and AVCS that aim to improve vehicle safe operation and vehicle driveability. The EKF and road friction estimation procedures evidence performance and robustness qualities necessary for incorporation in a commercial product. Simulation results show that parameters necessary for making and implementing intelligent driving decisions can be determined using these algorithms, and AVCS that incorporate filtering algorithms can potentially improve vehicle stability and handling qualities. Processing of field test data ranging from modest braking and pure steering inputs to extreme maneuvering provide additional evidence of reliable algorithm performance. The numerical technique for determining road friction works well for a variety of vehicle inputs ranging from normal (non emergency) stopping from highway speeds or turning and braking on a city road to inputs encountered during emergency maneuvers; however, for very small inputs, such as those that corresponding to a highway lane change or slow changes in velocity, tire forces are not large enough to determine road friction. Both simulation and field test data results show that the range of applicability of the EKF is not limited by the size of the tire forces, rather EKP performance is excellent for all maneuvers considered.

The results of this study have immediate application to the development of driver safety aids or warning devices in which control of a vehicle is not removed from the driver. Advanced vehicle control systems can also be developed based on the numerical procedures. The algorithms also have potential application to other cases not considered in this

study, including friction identification during traction, avoidance of driving on road surface where friction varies from side to side, and design of traction control systems.

INVESTIGATOR PROFILE

Laura R Ray received the B.S.E. and Ph.D. degrees in Mechanical and Aerospace Engineering from Princeton University in 1984 and 1991, respectively, and the M.S. degree from Stanford University in 1985. From 1990 to 1992 she was a faculty member of the Mechanical Engineering Department at Clemson University, and she has been a faculty member of the Mechanical Engineering Department at Christian Brothers University since 1993. Her research interests include applications of control and estimation theory to automotive, air transportation, and robotic systems, control system robustness, failure tolerant control, computer-aided control system design, mechatronics, and intelligent transportation systems. Dr. Ray has extensive experience in multivariable control system design, instrumentation, and microprocessor control of mechanical systems. She has authored or co-authored over twenty publications, including three on the subject presented in this report.

NOTES

1. VRTC measures road friction using standard ASTM procedures on a regular basis; however, the reliability of these data are questionable (*13*), and therefore, comparisons to these one-time measurements of road friction were not made in this project. Instead, general comparisons are made based on the results of a comprehensive road friction study given in (*14*).

2. Field test data for the braking maneuver and steering maneuver depicted in Fig. 4 and Fig. 2 1 contained a bad wheel angular velocity sensor on one of the rear wheels. Because wheel slip for this wheel could not be estimated accurately, the tire forces generated by this wheel were disregarded in the road friction estimation.

APPENDIX A: VEHICLE SIMULATION MODEL

An eight degree-of-freedom vehicle model *(9)* and an analytic tire force model *(10)* are used to simulate true motion from which noisy measurements are constructed. The equations of motion are

$$\dot{v}_x = v_y r + \frac{1}{m}(-m_s h\, r\, p + F_{xf} + F_{xr}) \tag{A.1}$$

$$\dot{v}_y = -v_x r + \frac{1}{m}(m_s h\, \dot{p} + F_{yf} + F_{yr}) \tag{A.2}$$

$$\dot{r} = (I_{xz}\dot{p} + F_{yf}L_f - F_{yr}L_r + (F_{xfl}\cos\delta_{fl} - F_{xfr}\cos\delta_{fr} + F_{yfl}\sin\delta_{fl} - F_{yfr}\sin\delta_{fr})\frac{t_f}{2} + (F_{xrl}\cos\delta_{rl} - F_{xrr}\cos\delta_{rr} + F_{yrl}\sin\delta_{rl} - F_{yrr}\sin\delta_{rr})\frac{t_r}{2} + M_z)\frac{1}{I_{zz}} \tag{A.3}$$

$$\dot{p} = (m_s h\,(\dot{v}_y + v_x r) + I_{xzs}\,\dot{r} + m_s h\, g\, \phi + M_q)\frac{1}{I_{xxs}} \tag{A.4}$$

$$\dot{\phi} = p \tag{A.5}$$

$$\dot{\omega}_{fl} = (F_{xfl}\, R_w - T_{fl})\frac{1}{I_w} \tag{A.6}$$

$$\dot{\omega}_{fr} = (F_{xfr}\, R_w - T_{fr})\frac{1}{I_w} \tag{A.7}$$

$$\dot{\omega}_{rl} = (F_{xrl}\, R_w - T_{rl})\frac{1}{I_w} \tag{A.8}$$

$$\dot{\omega}_{rr} = (F_{xrr}\, R_w - T_{rr})\frac{1}{I_w} \tag{A.9}$$

where

$$F_{xl} = -(F_{xfl}\cos\delta_{fl} + F_{xfr}\cos\delta_{fr}) - (F_{yfl}\sin\delta_{fl} + F_{yfr}\sin\delta_{fr}) \tag{A.10}$$

$$F_{yf} = -(F_{xfl}\sin\delta_{fl} + F_{xfr}\sin\delta_{fr}) + (F_{yfl}\cos\delta_{fl} + F_{yfr}\cos\delta_{fr}) \tag{A.11}$$

$$F_{xr} = -(F_{xrl}\cos\delta_{rl} + F_{xrr}\cos\delta_{rr}) - (F_{yrl}\sin\delta_{rl} + F_{yrr}\sin\delta_{rr}) \tag{A.12}$$

$$F_{yr} = -(F_{xrl}\sin\delta_{rl} + F_{xrr}\sin\delta_{rr}) + (F_{yrl}\cos\delta_{rl} + F_{yrr}\cos\delta_{rr}) \tag{A.13}$$

The state vector $\mathbf{x}(t)$ components are longitudinal and lateral velocity (v_x and v_y), yaw and roll rate (r and p), four wheel angular velocities (ω_{fl}, ω_{fr}, ω_{rl}, ω_{rr}) and roll angle (ϕ). $\mathbf{u}(t) = [\delta_{fl}\ \delta_{fr}\ \delta_{rl}\ \delta_{rr}\ T_{fl}\ T_{fr}\ T_{rl}\ T_{rr}]^T$ represents the steer angles and braking torques at each wheel. Components of the force vector $\mathbf{F}(t) = [F_{xfl}\ F_{xfr}\ F_{xrl}\ F_{xrr}\ F_{yfl}\ F_{yfr}\ F_{yrl}\ F_{yrr}\ M_Z]$ are longitudinal and lateral tire forces at each wheel and total tire restoring moment about the yaw axis. Sign conventions are defined in Fig. 5; the remaining parameters are given in Table 1. The analytic tire model generates tire forces and moments $\mathbf{F}(t)$ as a function of velocity, μ, and normal tire force, given a set of tire parameters *(10)*. The vehicle model also includes roll and compliance steer terms *(9)*. Roll steer is given by

$$\delta f = \delta f_0 + \varepsilon_f \phi, \quad \delta r = \varepsilon_r \phi \tag{A.14, A.15}$$

δf_0 represents the commanded front steer angle. Compliance steer introduces additional steering components to each wheel due to tire forces, moments, and suspension compliance. For example, the front wheel steer angles are

$$\delta_{fl} = \delta f + K_{yf} F_{yfl} + K_{xf} F_{xfl} + K_{mf} M_{zfl},\ \delta_{fr} = \delta f + K_{yf} F_{yfr} - K_{xf} F_{xfr} + K_{mf} M_{zfr} \tag{A.16,A.17}$$

where K_{xf}, K_{yf}, and K_{mf} are compliance steer coefficients due to front longitudinal force, lateral force, and restoring moments, respectively. Similar expressions exist for the δ_{rl} and δ_{rr}. The vehicle model includes first-order braking dynamics, with a time constant of 0.1 sec. For open-loop operation, a proportioning valve supplies 70% of T_b, the total brake torque, to the front wheels and 30% to the rear wheels in the vehicle simulation model.

An extended Kalman filter *(1)* is used to estimate the tire forces and vehicle state histories. The vehicle estimation model used by the filter includes the equations of motion, but requires no tire force model or knowledge of road

coefficient of friction. Instead, the state vector $\mathbf{x}(t)$ is augmented to include differential equations for each force to be estimated. Following *(3)*, an integrated random walk is chosen to model each force, allowing the forces to vary with time as necessary:

$$\begin{bmatrix} \dot{y}_0 \\ \dot{y}_1 \end{bmatrix} = \begin{bmatrix} 0 & 1 \\ 0 & 0 \end{bmatrix} \begin{bmatrix} y_0 \\ y_1 \end{bmatrix} + \mathbf{w}_y \tag{A.18}$$

y_0 represents the force to be estimated, y_1 is the first time derivatives of the force, and $\mathbf{w}_y$ is random, white noise. (Other higher-order Gauss-Markov models were evaluated, and good results were obtained for a variety of models.) Equation A.18 is appended to the state equations for each of the four longitudinal forces and two per-axle lateral forces, resulting in a 21st-order estimation model. Denoting the estimated variables as ($\hat{}$) and the nonlinear equations of motion as $\mathbf{f}(\mathbf{x}(t),\mathbf{F}(t),\mathbf{u}(t))$, the augmented nonlinear differential equation that models the system in the state estimator is

$$\dot{\hat{\mathbf{x}}}_{\mathbf{A}}(t) = \begin{bmatrix} \dot{\hat{\mathbf{x}}}(t) \\ \dot{\hat{\mathbf{F}}}(t) \end{bmatrix} = \begin{bmatrix} \mathbf{f}(\hat{\mathbf{x}}(t), \hat{\mathbf{F}}(t), \mathbf{u}(t)) \\ \mathbf{A}\,\hat{\mathbf{F}}(t) \end{bmatrix} = \mathbf{f}_{\mathbf{A}}(\hat{\mathbf{x}}_{\mathbf{A}}(t), \mathbf{u}(t)) \tag{A.19}$$

where $\mathbf{A}$ is a block-diagonal matrix with blocks defined by the matrix in eq. A.18, and $\hat{\mathbf{x}}_{\mathbf{A}}(t)$ is the augmented state vector. Tire restoring moment is neglected in the estimation model. The estimation model retains roll and compliance steer terms given above. In addition to steering and braking inputs, the vehicle is assumed to be subject to Gaussian, white disturbance. The nonlinear measurement equation used by the extended Kalman filter is

$$\mathbf{z}(t) = [r \;\; p \;\; \omega_{fl} \;\; \omega_{fr} \;\; \omega_{rl} \;\; \omega_{rr} \;\; a_x \;\; a_y]^T = \mathbf{h}[\mathbf{x}(t),\mathbf{F}(t),\mathbf{u}(t))] + \mathbf{n}(t) \tag{A.20}$$

where a_x and a_y are the longitudinal and lateral accelerations, respectively, and $\mathbf{n}(t)$ is Gaussian, white measurement noise. Sensors are contained on the vehicle, and the set includes readily available sensors, such as accelerometers, rate gyros, and tachometers. In addition, it is assumed that the control inputs are measured. A hybrid extended Kalman filter is implemented by integrating eq. A.20 and a continuous-time matrix Riccati equation from time t_{k-1} to time t_k to propagate the state and error covariance ($\mathbf{P}$) estimates, computing the filter gain matrix, and updating the state and covariance estimates based on the measurement residual *(1)*:

$$\hat{\mathbf{x}}_{\mathbf{A}k}(-) = \hat{\mathbf{x}}_{\mathbf{A}k-1}(+) + \int_{t_{k-1}}^{t_k} \mathbf{f}_{\mathbf{A}}(\hat{\mathbf{x}}_{\mathbf{A}}(\tau), \mathbf{u}(\tau))d\tau \tag{A.21}$$

$$\mathbf{P}_k(-) = \mathbf{P}_{k-1}(+) + \int_{t_{k-1}}^{t_k} \{\mathbf{F}(\tau)\mathbf{P}(\tau) + \mathbf{P}(\tau)\mathbf{F}^{\mathbf{T}}(\tau) + \mathbf{L}AV(\tau)\mathbf{L}^{\mathbf{T}}\}d\tau \tag{A.22}$$

$$\mathbf{K}_k = \mathbf{P}_k(-)\mathbf{H}_k^{\mathbf{T}}\,[\mathbf{H}_k\,\mathbf{P}_k(-)\mathbf{H}_k^{\mathbf{T}} + \mathbf{R}_k]^{-1} \tag{A.23}$$

$$\hat{\mathbf{x}}_{\mathbf{A}k}(+) = \hat{\mathbf{x}}_{\mathbf{A}k}(-) + \mathbf{K}_k\,[\mathbf{z}_k - \mathbf{h}_{\mathbf{A}}(\hat{\mathbf{x}}_{\mathbf{A}k}(-),\mathbf{u}(t))] \tag{A.24}$$

$$\mathbf{P}_k(+) = [\mathbf{I} - \mathbf{K}_k\,\mathbf{H}_k\,]\mathbf{P}_k(-) \tag{A.25}$$

Nonlinear integration procedures are implemented using fourth-order Runge Kutta integration. Matrices $\mathbf{F}$ and $\mathbf{H}$ are computed by linearizing eq. A.19-A.20 around $\hat{\mathbf{x}}_{\mathbf{A}k}(-)$ at each time step. The disturbance input matrix, $\mathbf{L}$, is constant, since the disturbances enter linearly. The equations governing the tire forces in the estimation model are driven by the measurement residual $[\mathbf{z}_k - \mathbf{h}(\hat{\mathbf{x}}_{\mathbf{A}k}(-),\mathbf{u}(t))]$ in eq. A.24. The EKF is initialized with a state estimate corresponding to the true state and a large covariance matrix. Slip and slip angle estimates are derived from the state estimate for use in road friction identification and/or feedback control laws.

REFERENCES

1. R.F. Stengel. *Stochastic Optimal Control: Theory and Application.* John Wiley and Sons, New York, 1986.

2. H.L. Salford. High-alpha aerodynamic model identification of T-2C aircraft using the EBM method. *Journal of Aircraft*, vol. 18, no. 10, Oct. 1981, pp. 801-809.

3. M. Sri-Jayantha and R.F. Stengel. Determination of nonlinear aerodynamic coefficients using the estimation-before-modeling method. *Journal of Aircraft*, vol. 25, no. 9, Sept. 198, pp. 796-804.

4. A. Niehaus and Stengel, R. Rule-Based Guidance for Highway Driving in the Presence of Uncertainty, *ASME Journal of Dynamic Systems, Measurement , and Control*, Vol.116, Dec. 1994, pp. 668-674.

5. Niehaus, A., and R.F. Stengel. Probability-Based Decision Making for Automated Highway Driving. *Proceedings of the 1991 International Control Conference on Vehicle Navigation and Information Systems*, Dearborn, Michigan, October 1991.

6. S. Taheri and E.H. Law. Investigation of a combined slip control braking and closed-loop four wheel steering system for an automobile during combined hard braking and steering. *Proceedings of the 1990 American Control Conference*, San Diego, CA, 1990.

7. S. Kimbrough. A Brake Control Strategy for Emergency Stops that Involve Steering, *Procesedings of the ASME Symposium on Transportation Systems,* Dallas, Texas, Nov 1990, pp. 117-129.

8. D.L. Margolis and M. Tran. Integrated Torque and Steering Control for Improved Vehicle Handling, *Procesedings of the 1991 ASME Symposium on Transportation Systems*, Atlanta, GA, Dec 1991, pp. 267-290.

9. C.J. Constantine, J.E. Bowman and E.H. Law. *Development of Models and Computer Programs for Lateral Dynamics of Automobiles During Combined Steering and Braking Maneuvers.* TR-90-132-ME-MMS, Mechanical Engineering Department, Clemson University, June 1991.

10. H.T. Szostak, R.W. Allen, and T.J. Rosenthal. *Analytical Modeling of a Driver Response in Crash Avoidance Maneuvering Vol II: An Interactive Tire Model for Driver/Vehicle Simulation.* U.S. Department of Transportation, Report No. DOT HS 807-271, April 1988.

11. MATLAB Reference Guide, The MathWorks, Natick, MA, August, 1992.

12. L.R. Ray. Nonlinear State and Tire Force Estimation for Advanced Vehicle Control. *IEEE Transactions on Control Systems Technology*, Vol. 3, No. 1, Mar 1995, pp. 117-124.

13. Mr. Jeff Chrstos, Vehicle Research and test Center, East Liberty, Ohio, Private Communication.

14. N. Elbert. SAE Tire Braking Traction Survey: A Comparison of Public Highways and Test Surfaces. SAE Paper No. 890638 Feb. 1989.

15. L.R. Ray. Real-Time Determination of Road Coefficient of Friction for ITS and Advanced Vehicle Control. *Proceedings of the 1995 American Control Conference*, Seattle, WA, pp. 2133-2138, June 1995.

16. L.R. Ray. Stochastic Decision and Control Parameters for ITS. *to appear in the proceedings of the 1995 ASME International Mechanical Engineering Congress and Exposition*, San Francisco CA, Nov 1995.

17. L.R. Ray. Nonlinear Tire Force Estimation and Road Friction Identification: Field Test Results. *to appear in the Proceedings of the 1996 SAE Congress*, Feb 1996.

18 Mr. Doug Pape, Battelle Memorial Institute, Columbus, OH, Private Communication re: Contract DTNH22-93-C-07023, "Run-off-road collision avoidance using ITS countermeasures."

LIST OF FIGURES

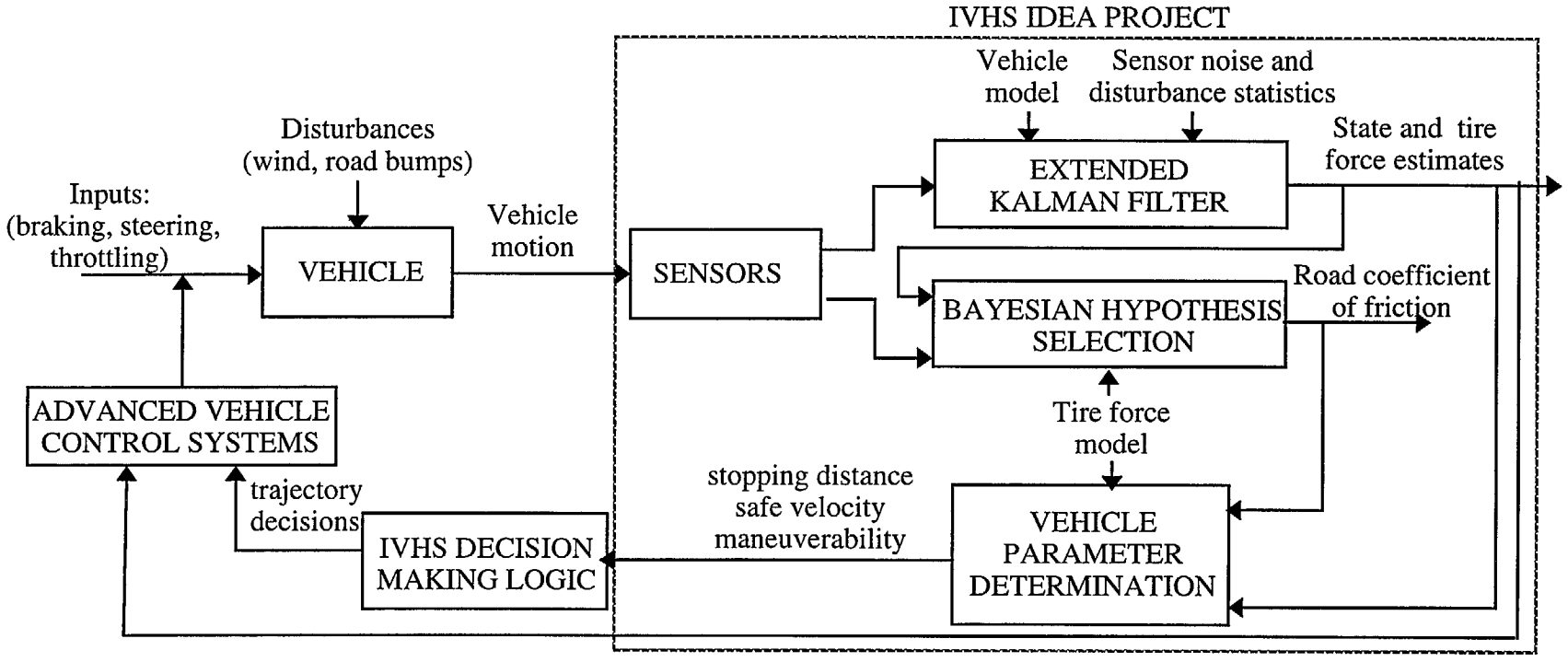
IVHS IDEA PROJECT
Vehicle model
Sensor noise and disturbance statistics
Disturbances (wind, road bumps)
Inputs: (braking, steering, throttling)
VEHICLE
Vehicle motion
SENSORS
EXTENDED KALMAN FILTER
State and tire force estimates
BAYESIAN HYPOTHESIS SELECTION
Road coefficient of friction
Tire force model
ADVANCED VEHICLE CONTROL SYSTEMS
trajectory decisions
IVHS DECISION MAKING LOGIC
stopping distance safe velocity maneuverability
VEHICLE PARAMETER DETERMINATION

Figure 1

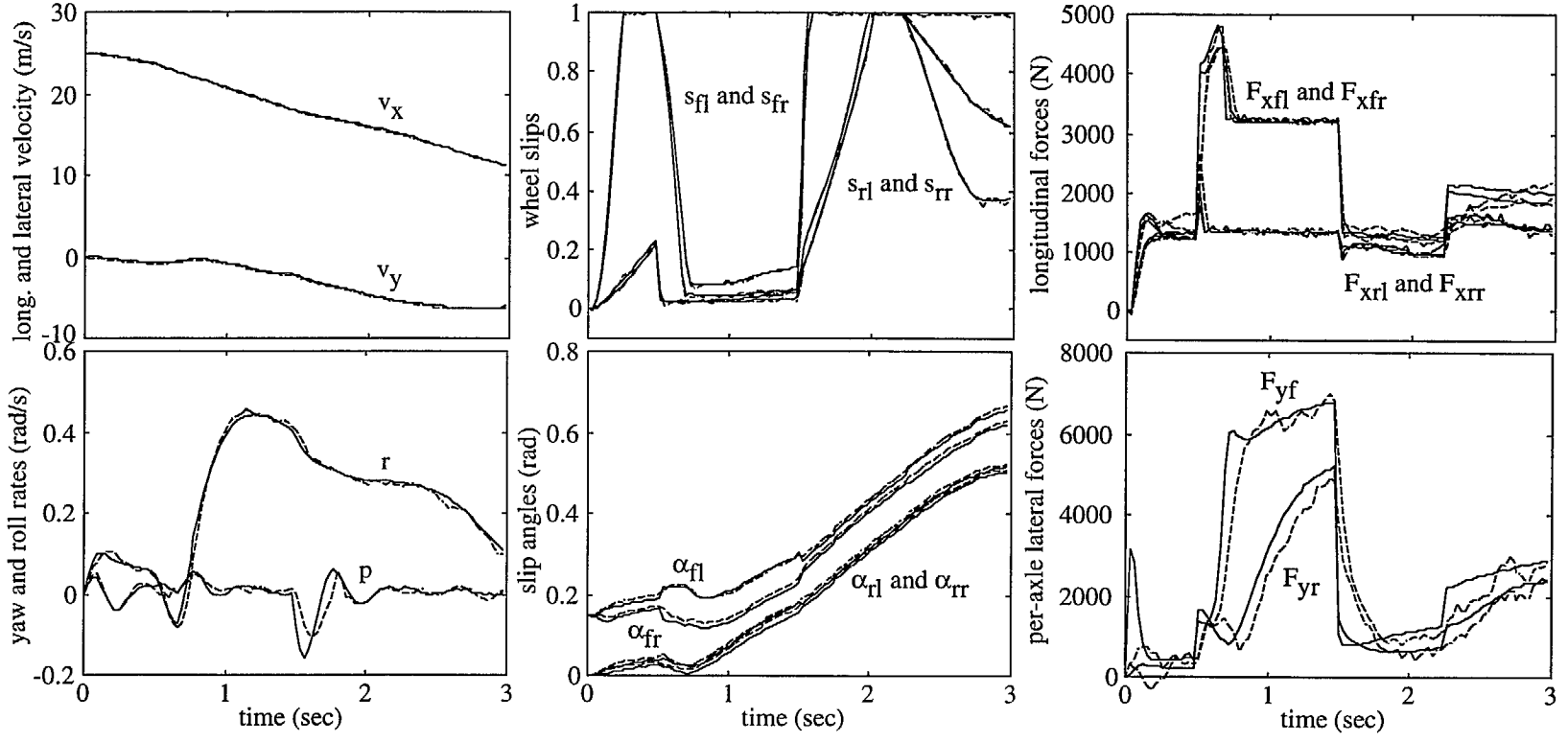
long. and lateral velocity (m/s)
30
20
10
0
-10
v_x
v_y
wheel slips
1
0.8
0.6
0.4
0.2
0
s_{fl} and s_{fr}
s_{rl} and s_{rr}
longitudinal forces (N)
5000
4000
3000
2000
1000
0
F_{xfl} and F_{xfr}
F_{xrl} and F_{xrr}
yaw and roll rates (rad/s)
0.6
0.4
0.2
0
-0.2
r
p
slip angles (rad)
0.8
0.6
0.4
0.2
0
α_{fl}
α_{fr}
α_{rl} and α_{rr}
per-axle lateral forces (N)
8000
6000
4000
2000
0
F_{yf}
F_{yr}
0
1
2
3
time (sec)

Figure 2

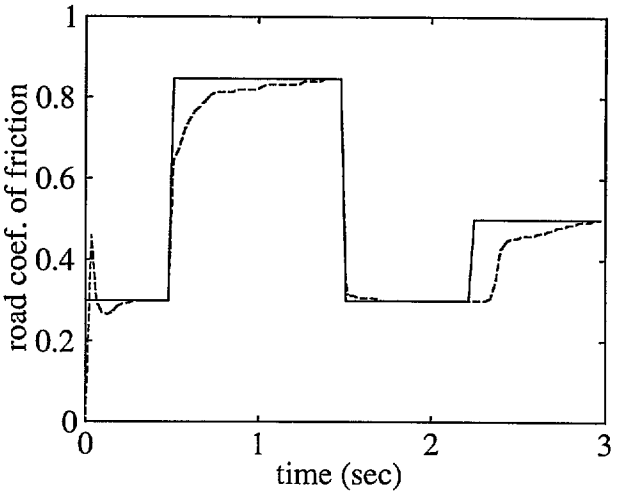

Figure 3

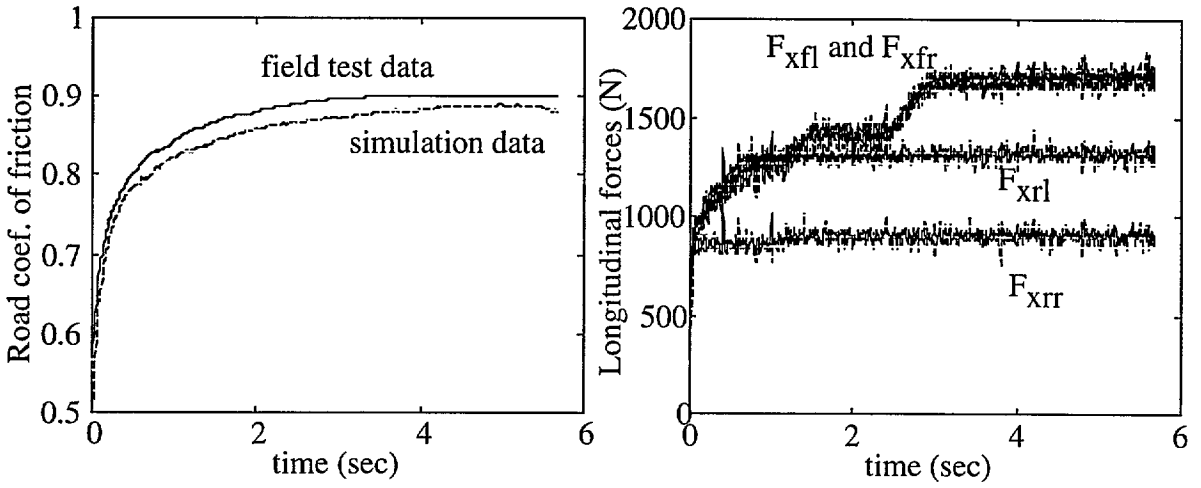
Road coef. of friction
field test data
simulation data
time (sec)
Longitudinal forces (N)
F_{xfl} and F_{xfr}
F_{xrl}
F_{xrr}
time (sec)

Figure 4

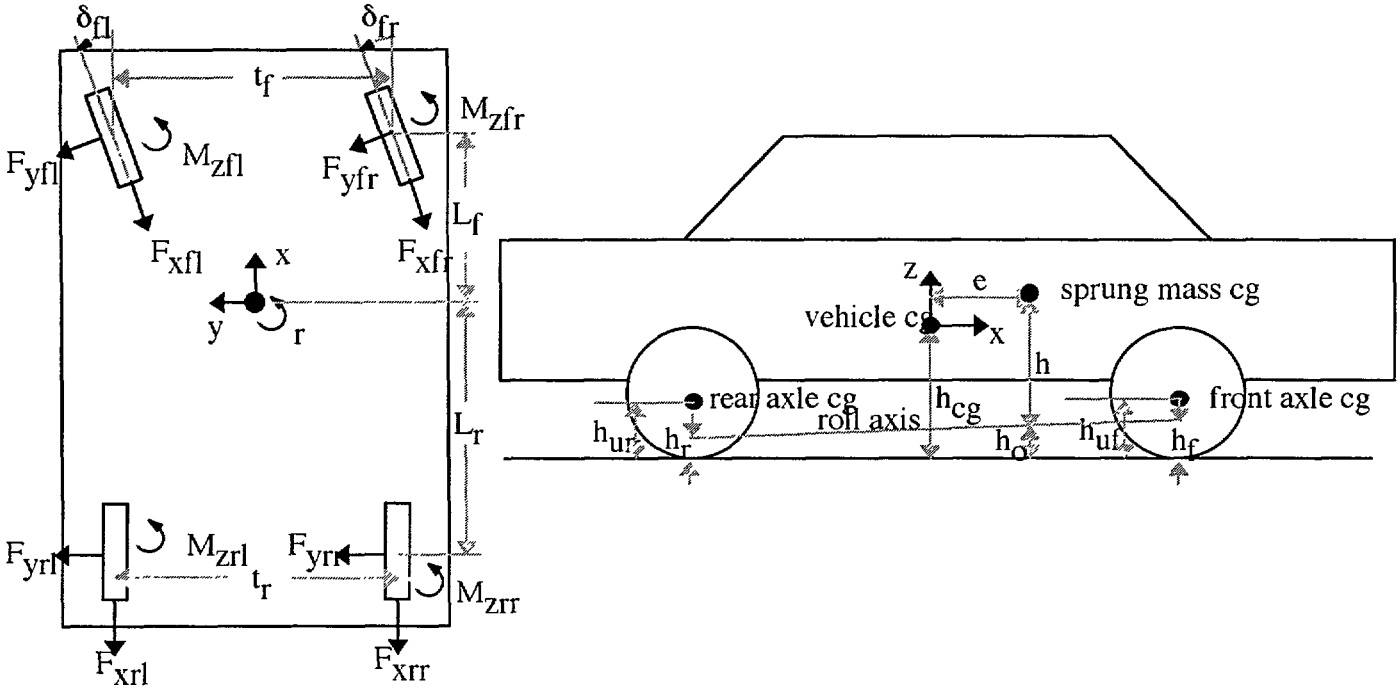
δfl
δfr
tf
Mzfr
Fyfl
Mzfl
Fyfr
Lf
Fxfl
Fxfr
x
y
r
Lr
Fyrl
Mzrl
Fyrr
tr
Mzrr
Fxrl
Fxrr
z
e
sprung mass cg
vehicle cg
x
h
rear axle cg
roll axis
hcg
front axle cg
hur
hr
hcf
huf
hf

Figure 5

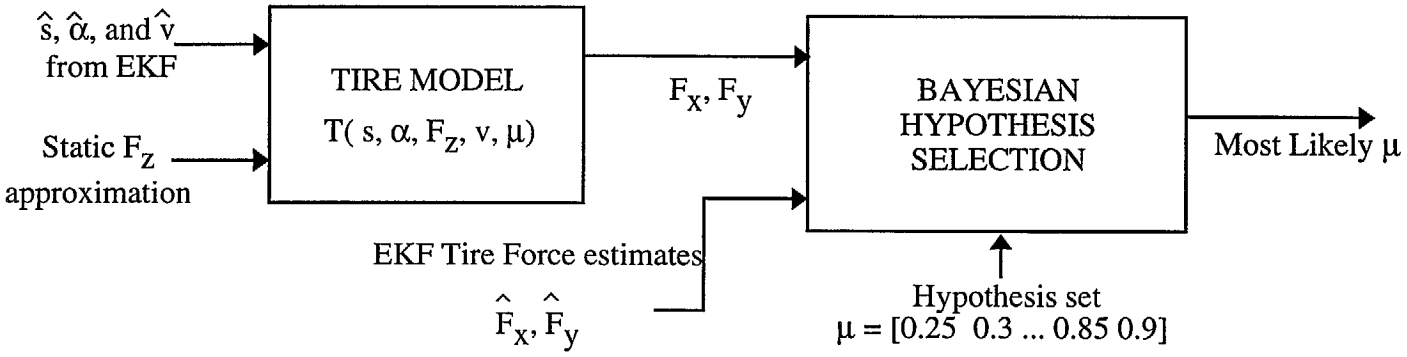
$\hat{s}$, $\hat{\alpha}$, and $\hat{v}$
from EKF
Static F_z
approximation
TIRE MODEL
T(s, α, F_z, v, μ)
F_x, F_y
BAYESIAN
HYPOTHESIS
SELECTION
Most Likely μ
EKF Tire Force estimates
$\hat{F}_x$, $\hat{F}_y$
Hypothesis set
μ = [0.25 0.3 ... 0.85 0.9]

Figure 6

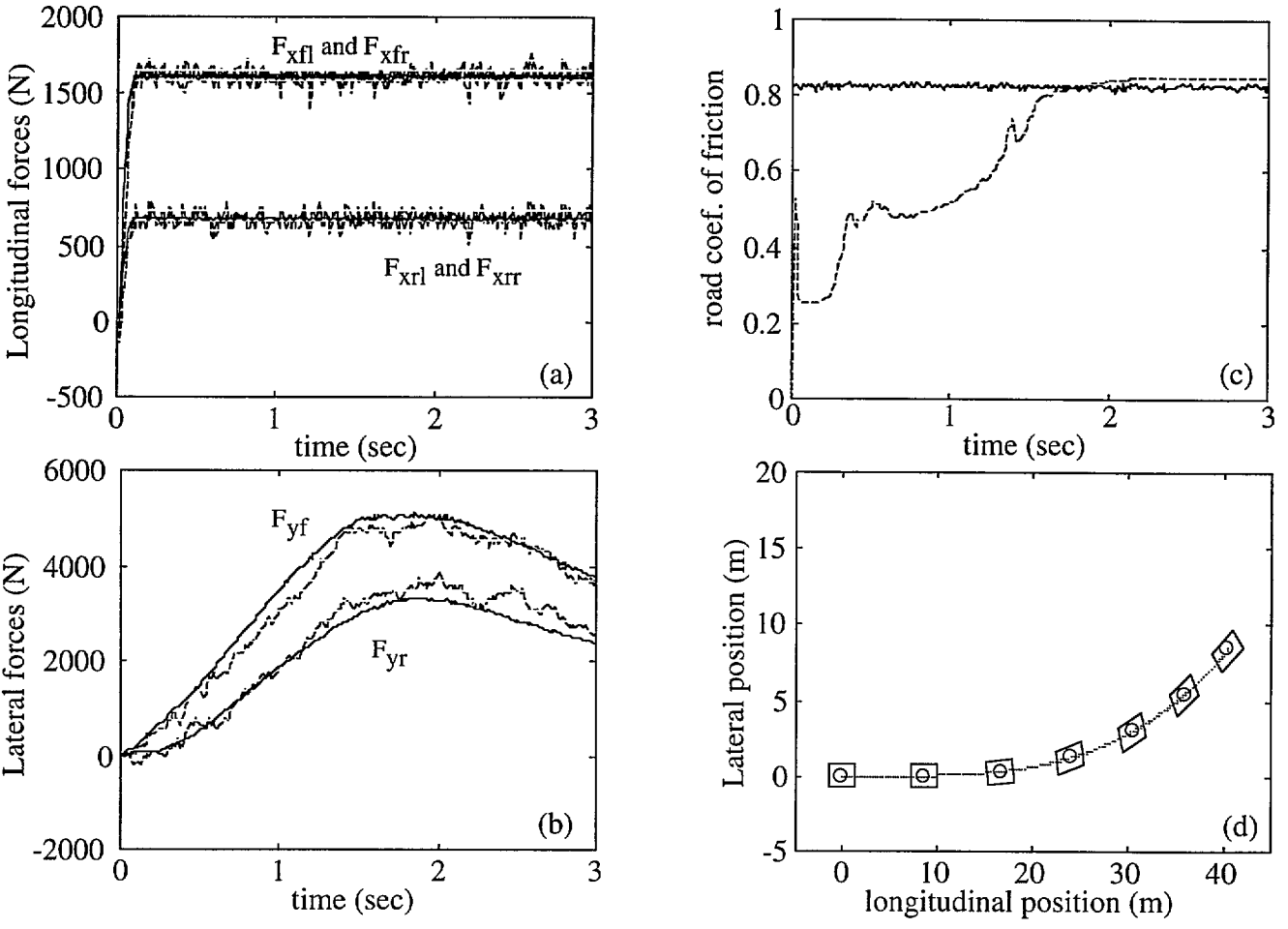
Longitudinal forces (N)
2000
1500
1000
500
0
-500
F_{xfl} and F_{xfr}
F_{xrl} and F_{xrr}
(a)
0
1
2
3
time (sec)
road coef. of friction
1
0.8
0.6
0.4
0.2
0
(c)
time (sec)
Lateral forces (N)
6000
4000
2000
0
-2000
F_{yf}
F_{yr}
(b)
time (sec)
Lateral position (m)
20
15
10
5
0
-5
(d)
0
10
20
30
40
longitudinal position (m)

Figure 7

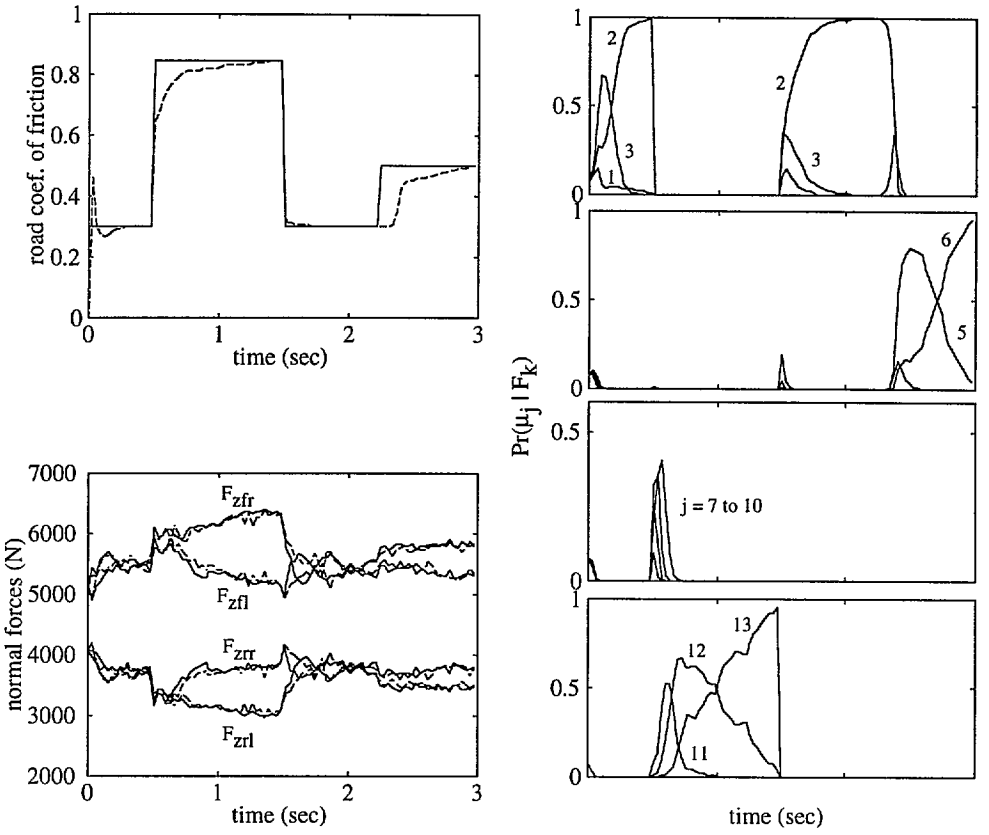
road coef. of friction
time (sec)
normal forces (N)
F_{zfr}
F_{zfl}
F_{zrr}
F_{zrl}
time (sec)
$Pr(\mu_j \mid F_k)$
2
3
1
2
3
6
5
j = 7 to 10
13
12
11
time (sec)

Figure 8

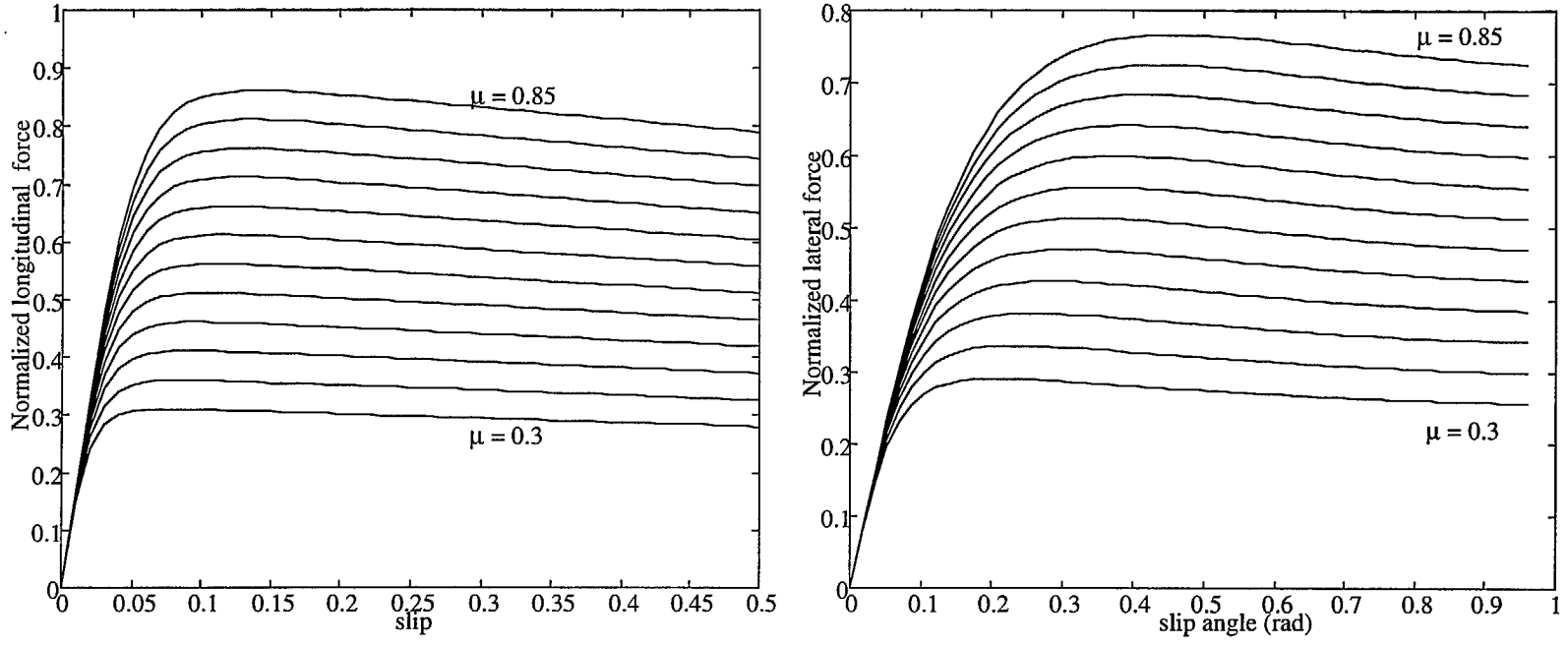
Normalized longitudinal force
slip
μ = 0.85
μ = 0.3
Normalized lateral force
slip angle (rad)
μ = 0.85
μ = 0.3

Figure 9

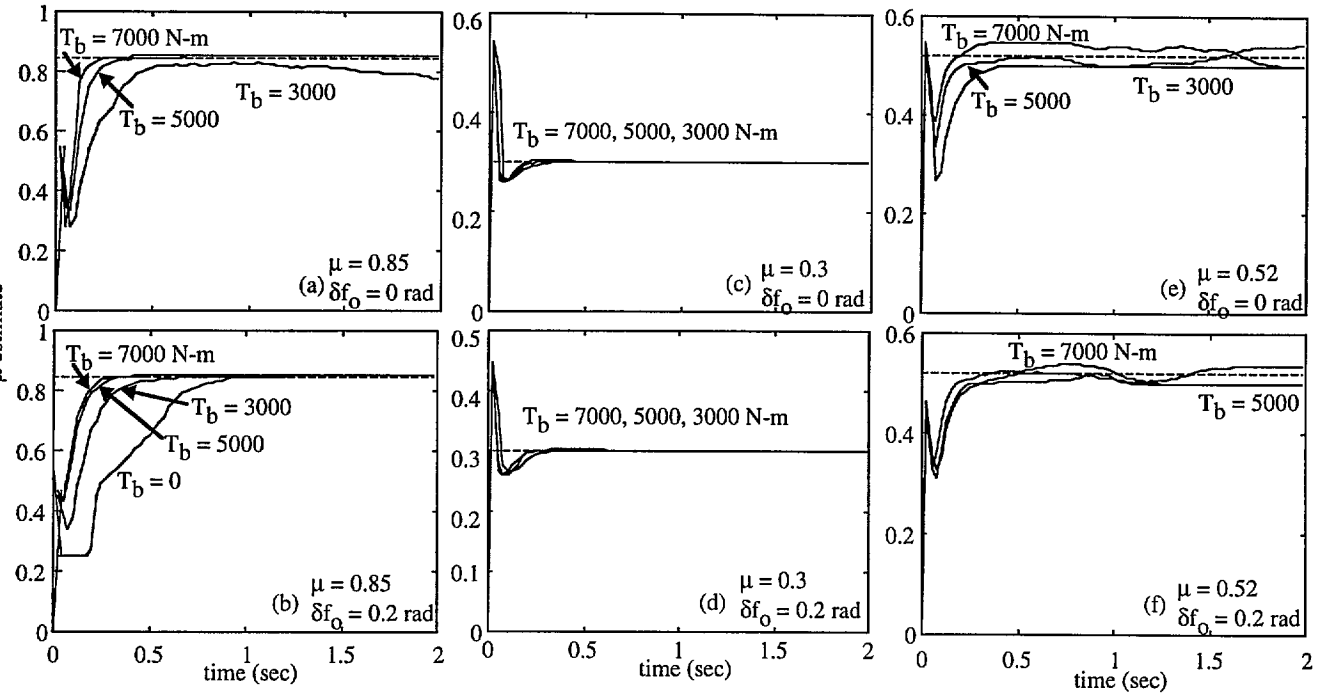
T_b = 7000 N-m
T_b = 3000
T_b = 5000
μ = 0.85
(a) δf_o = 0 rad
T_b = 7000, 5000, 3000 N-m
μ = 0.3
(c) δf_o = 0 rad
T_b = 7000 N-m
T_b = 5000
T_b = 3000
μ = 0.52
(e) δf_o = 0 rad
T_b = 7000 N-m
T_b = 3000
T_b = 5000
T_b = 0
μ = 0.85
(b) δf_o = 0.2 rad
T_b = 7000, 5000, 3000 N-m
μ = 0.3
(d) δf_o = 0.2 rad
T_b = 7000 N-m
T_b = 5000
μ = 0.52
(f) δf_o = 0.2 rad
time (sec)
time (sec)
time (sec)

Figure 10

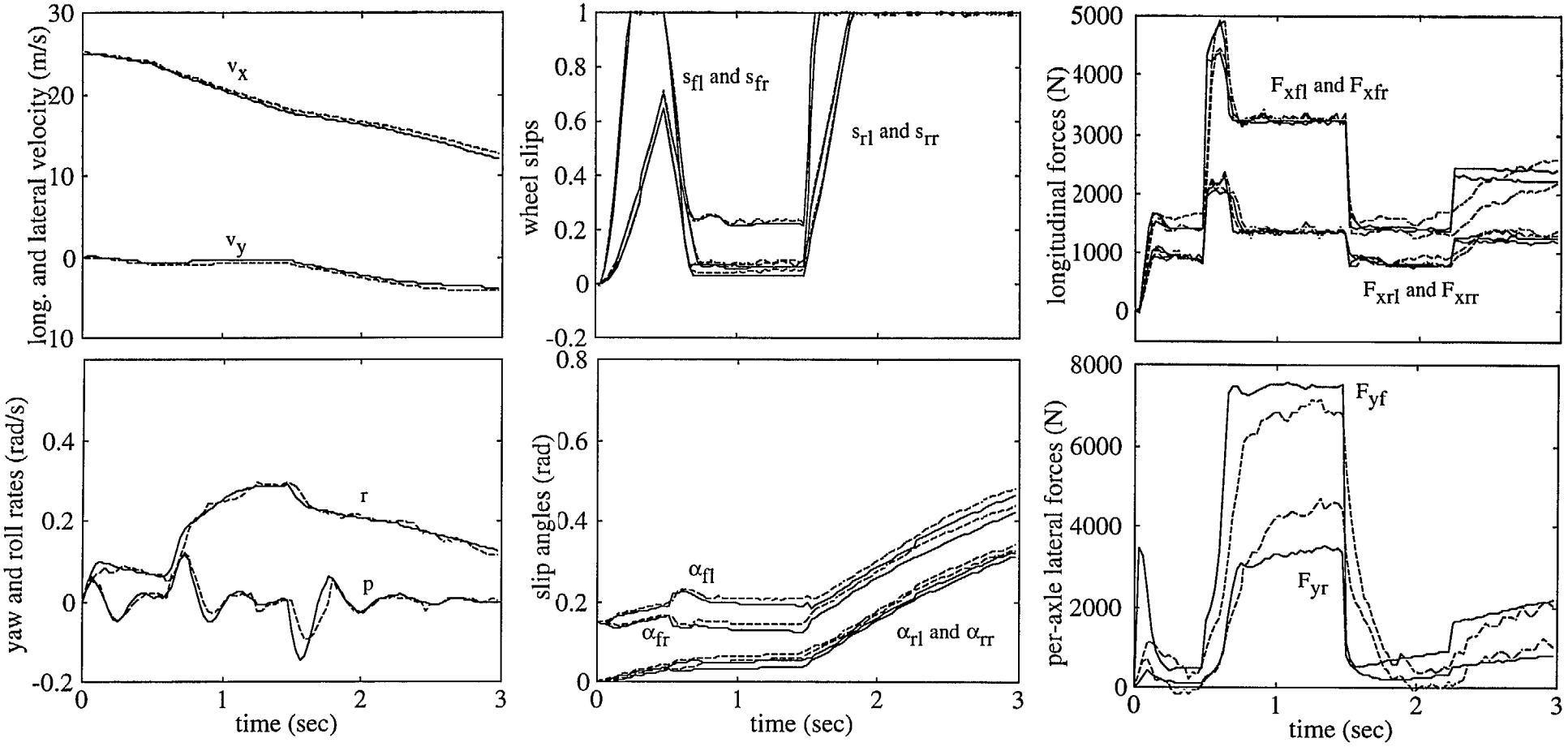

Figure 11 Actual motion (solid lines) and estimated motion from an extended Kalman filter (dashed lines) with model uncertainty

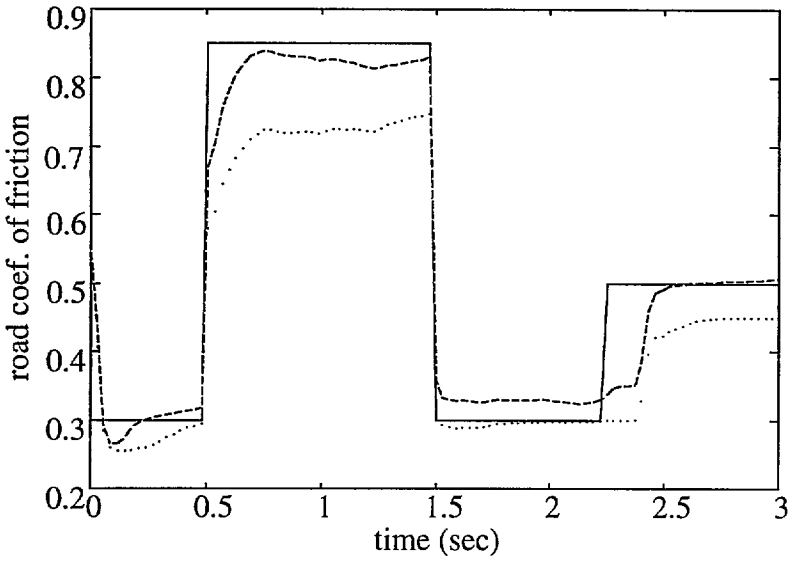
0.9
0.8
0.7
0.6
0.5
0.4
0.3
0.2
road coef. of friction
0
0.5
1
1.5
2
2.5
3
time (sec)

Figure 12

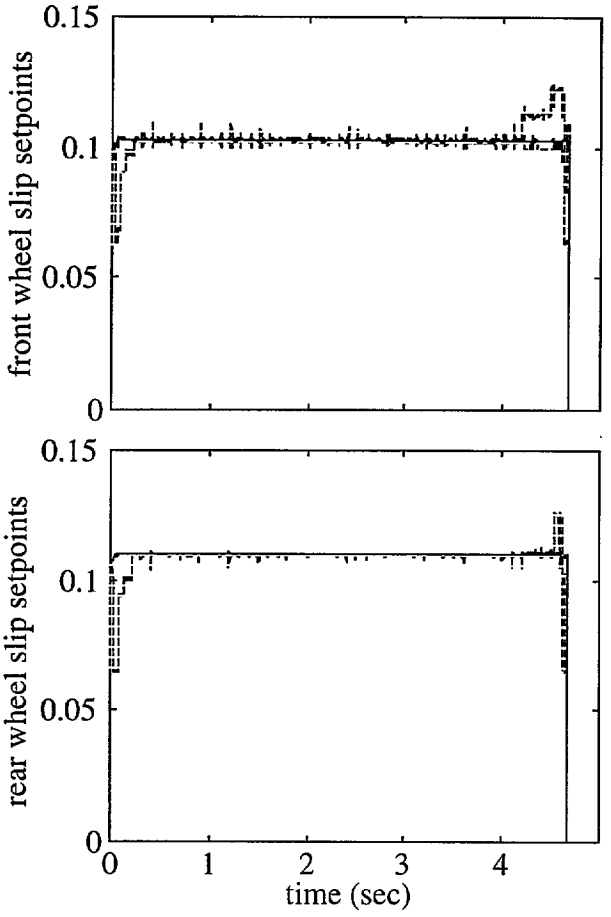
0.15
0.1
0.05
0
front wheel slip setpoints
0.15
0.1
0.05
0
rear wheel slip setpoints
0
1
2
3
4
time (sec)

Figure 13

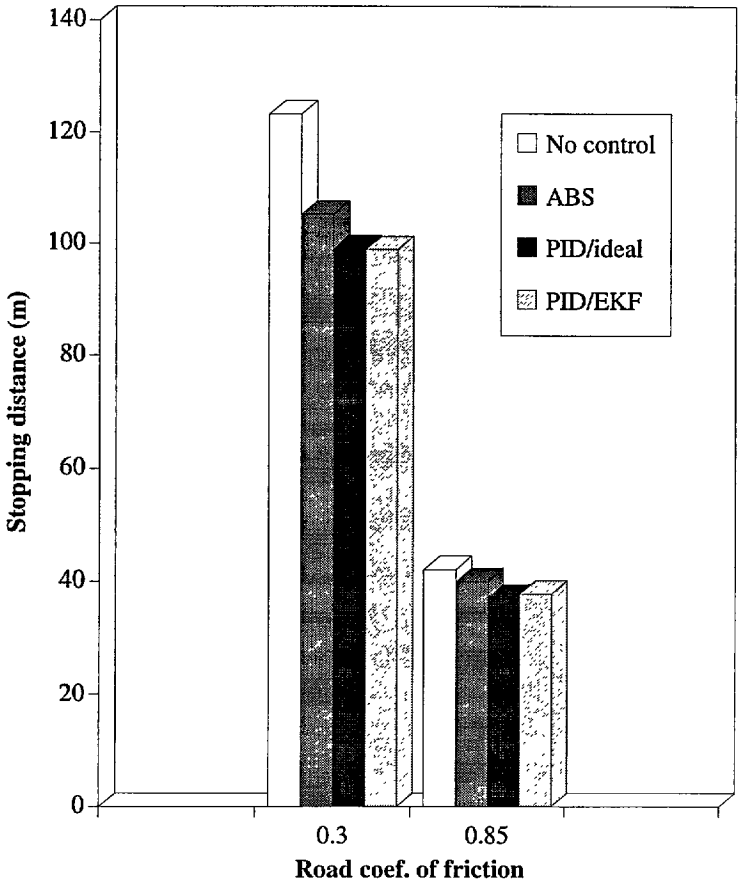
140
120
100
80
60
40
20
0
Stopping distance (m)
No control
ABS
PID/ideal
PID/EKF
0.3
0.85
Road coef. of friction

Figure 14

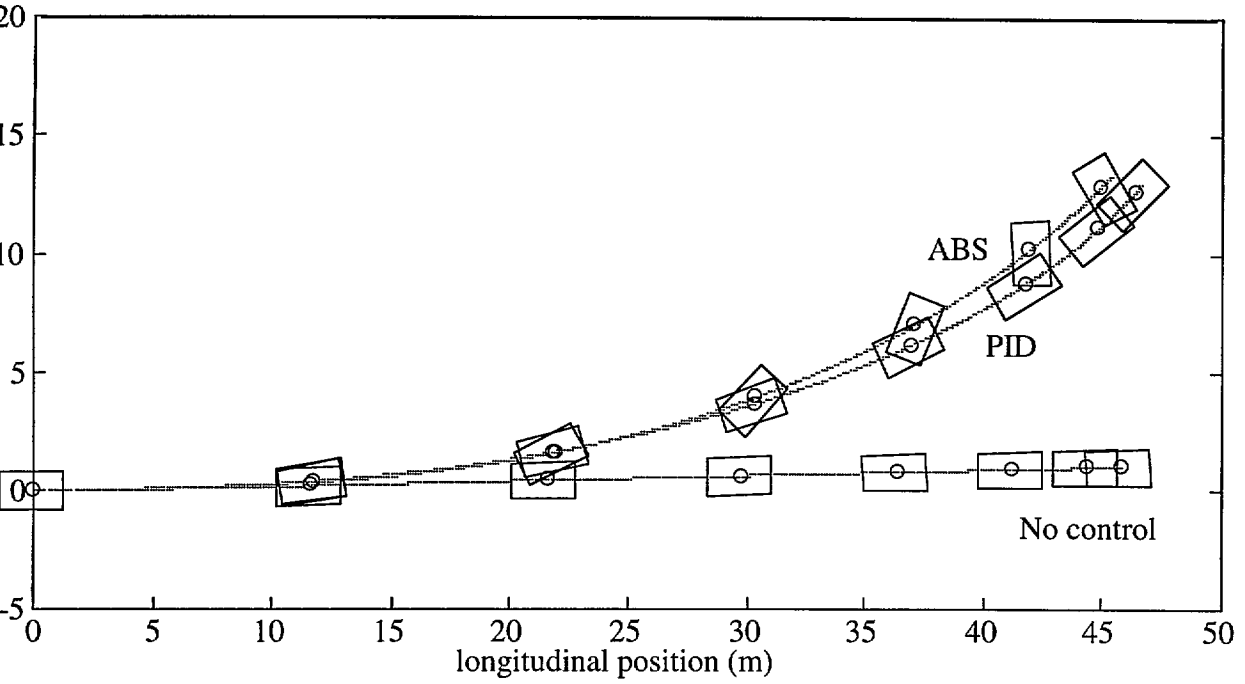
ABS
PID
No control
longitudinal position (m)

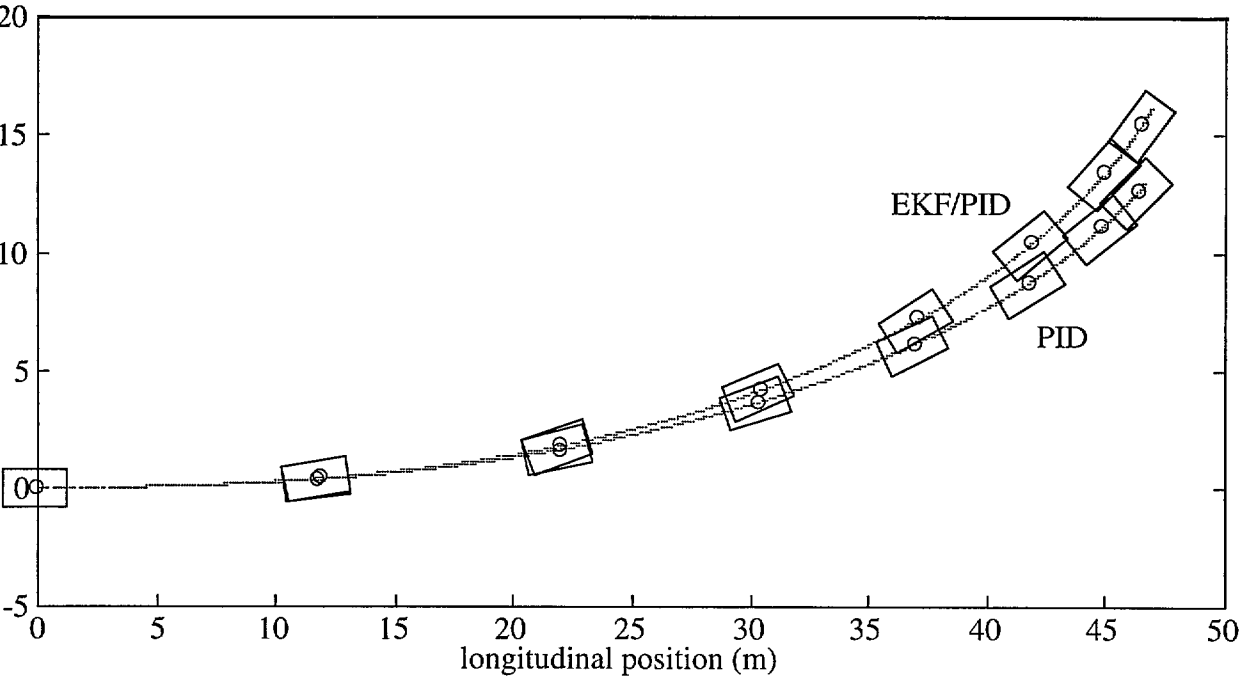
EKF/PID
PID
longitudinal position (m)

Figure 15

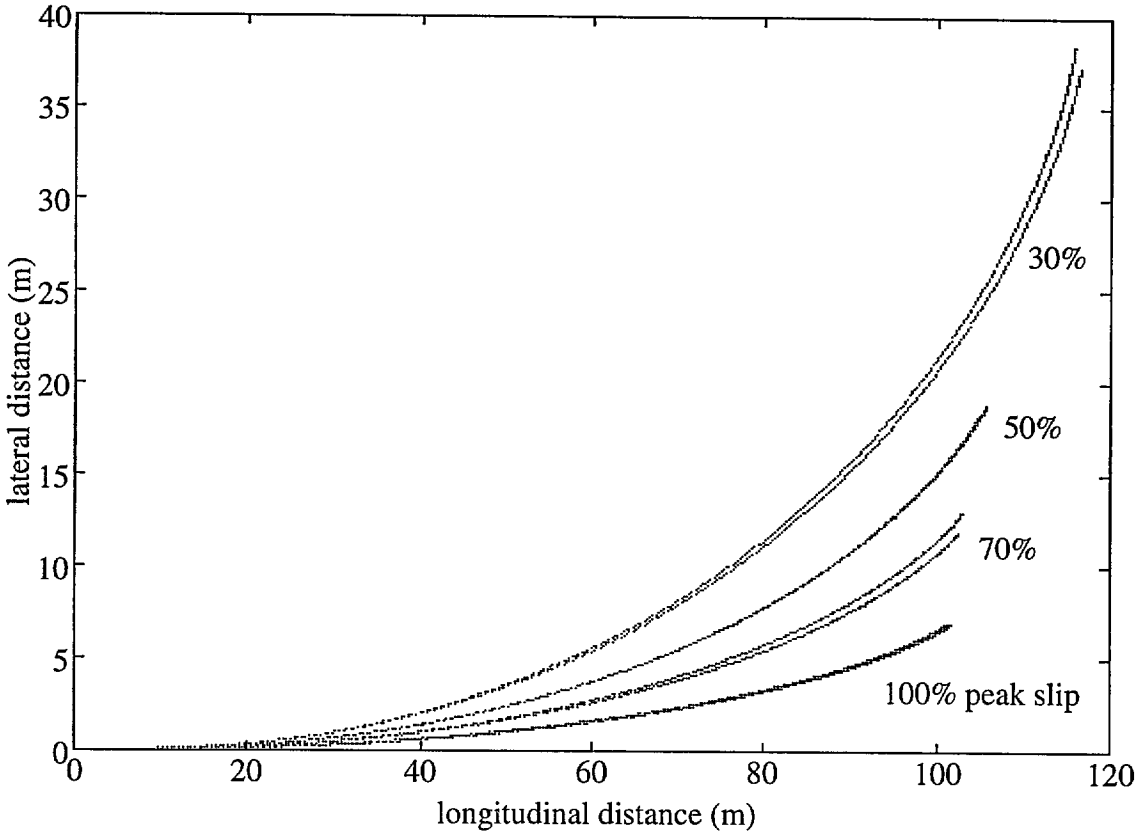
lateral distance (m)
longitudinal distance (m)
30%
50%
70%
100% peak slip

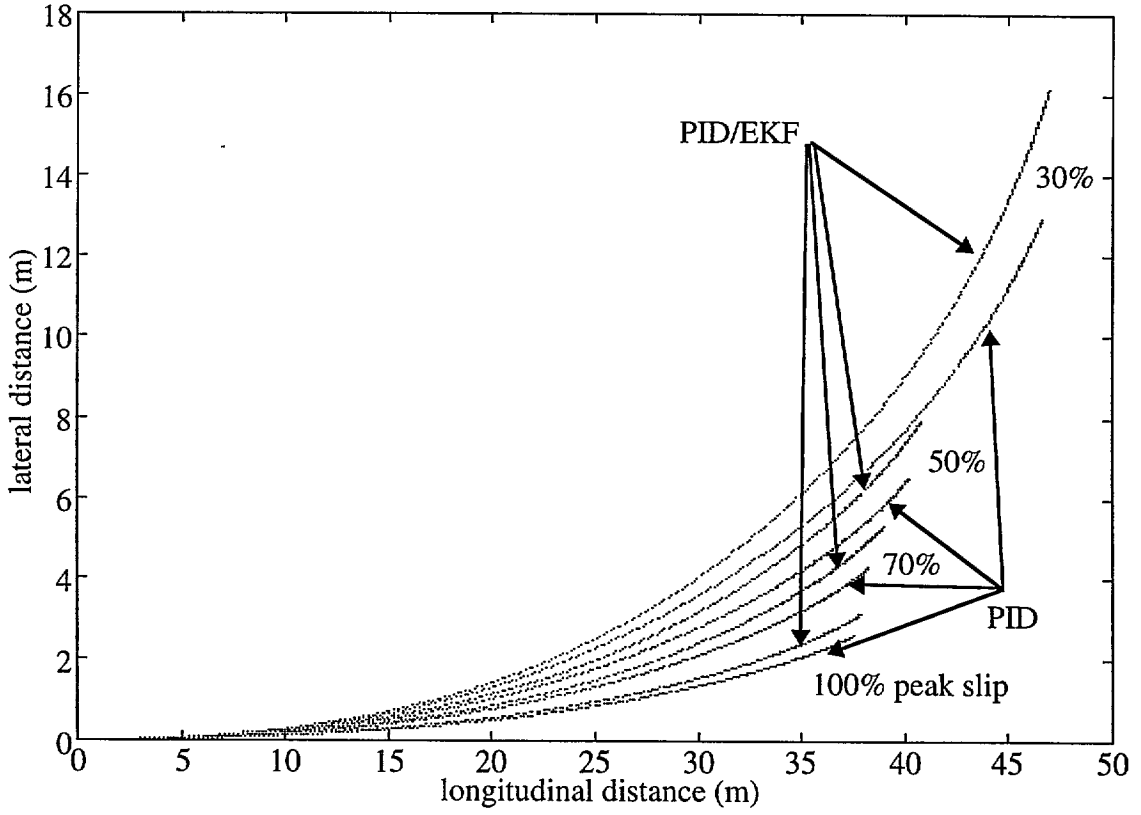
lateral distance (m)
longitudinal distance (m)
PID/EKF
30%
50%
70%
PID
100% peak slip

Figure 16

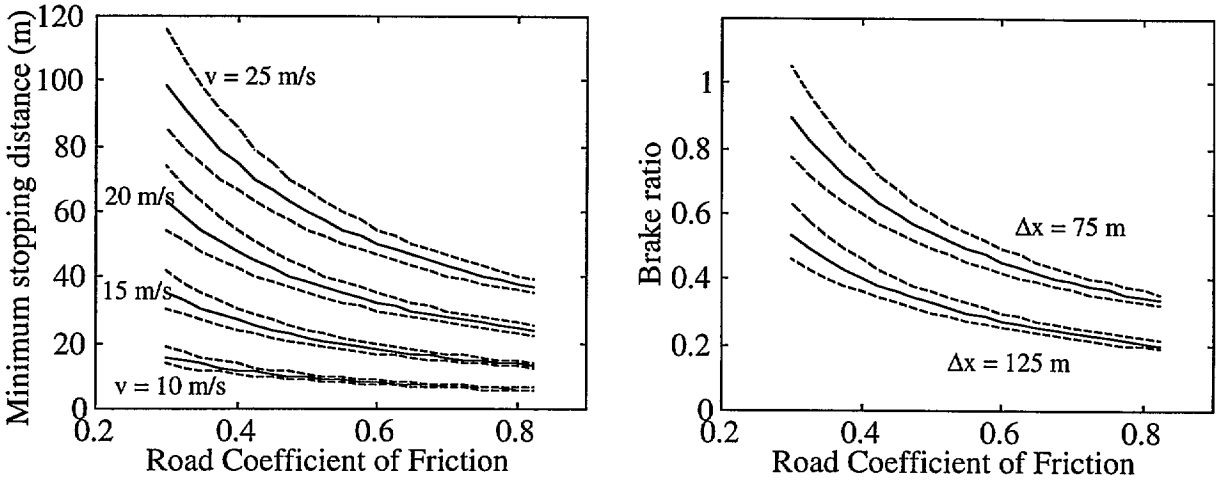
Minimum stopping distance (m)
120
100
80
60
40
20
0
v = 25 m/s
20 m/s
15 m/s
v = 10 m/s
0.2
0.4
0.6
0.8
Road Coefficient of Friction
Brake ratio
1
0.8
0.6
0.4
0.2
0
Δx = 75 m
Δx = 125 m
0.2
0.4
0.6
0.8
Road Coefficient of Friction

Figure 17

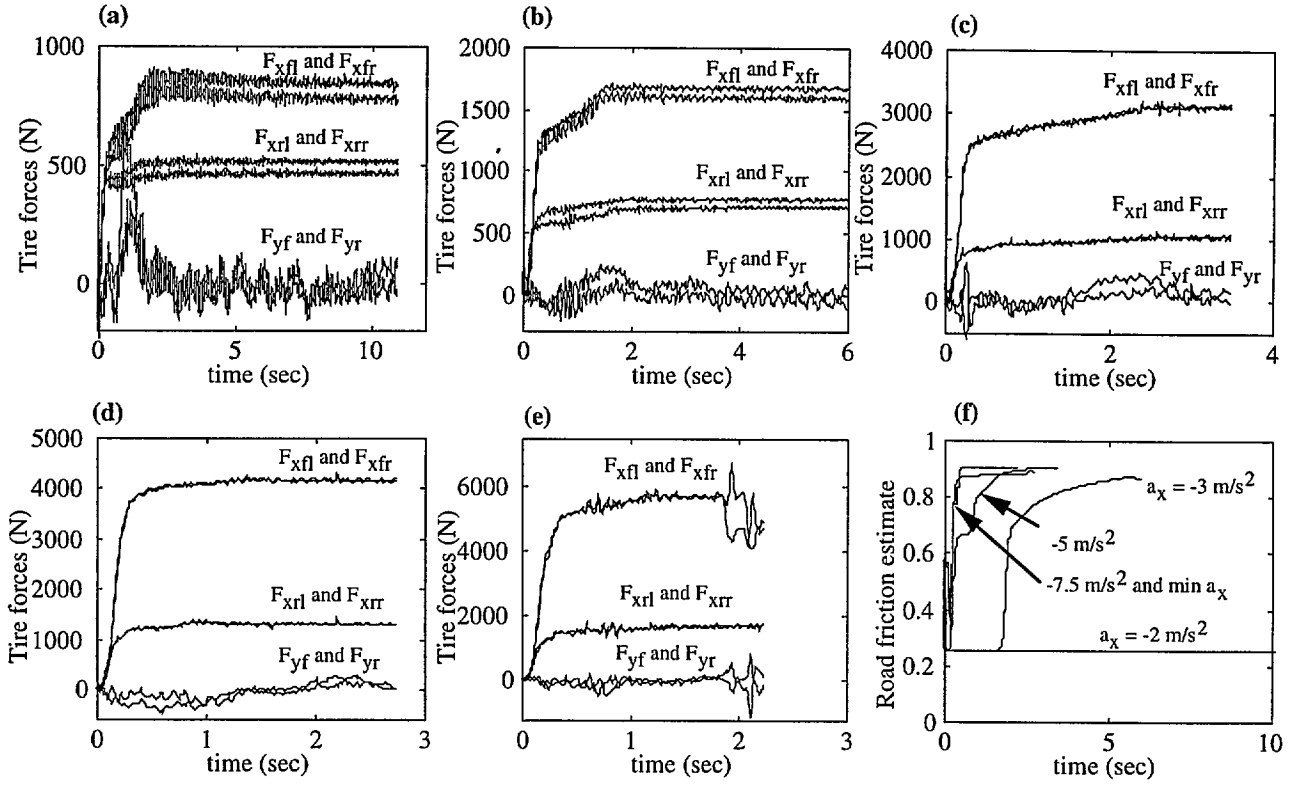
(a)
(b)
(c)
(d)
(e)
(f)
Tire forces (N)
Road friction estimate
time (sec)
F_{xfl} and F_{xfr}
F_{xrl} and F_{xrr}
F_{yf} and F_{yr}
a_x = -3 m/s^2
-5 m/s^2
-7.5 m/s^2 and min a_x
a_x = -2 m/s^2

Figure 18

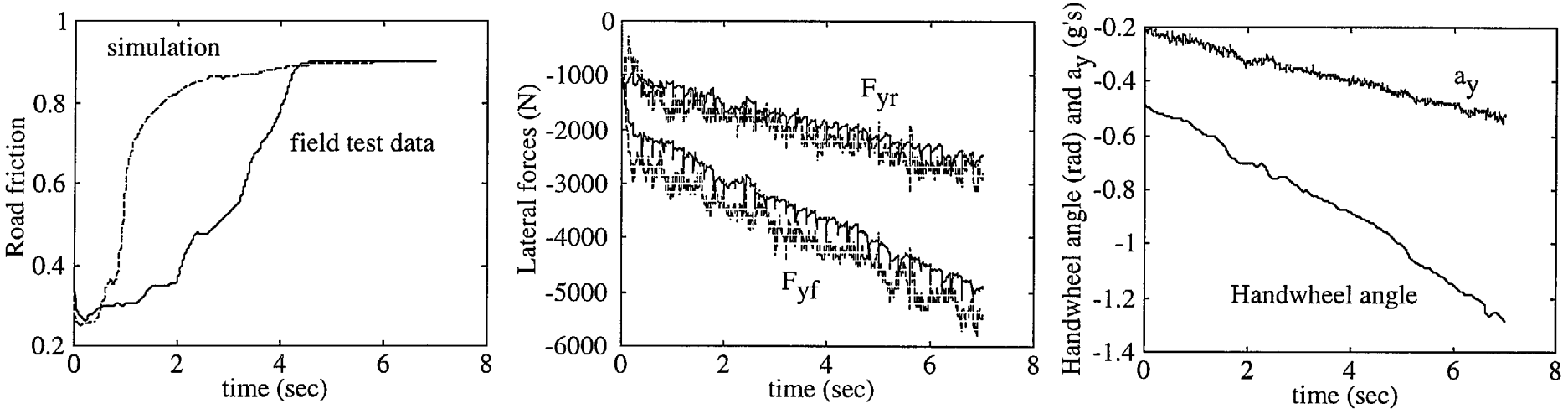
simulation
field test data
Road friction
time (sec)
Lateral forces (N)
F_{yr}
F_{yf}
time (sec)
Handwheel angle (rad) and a_y (g's)
a_y
Handwheel angle
time (sec)

Figure ~~18~~ 19

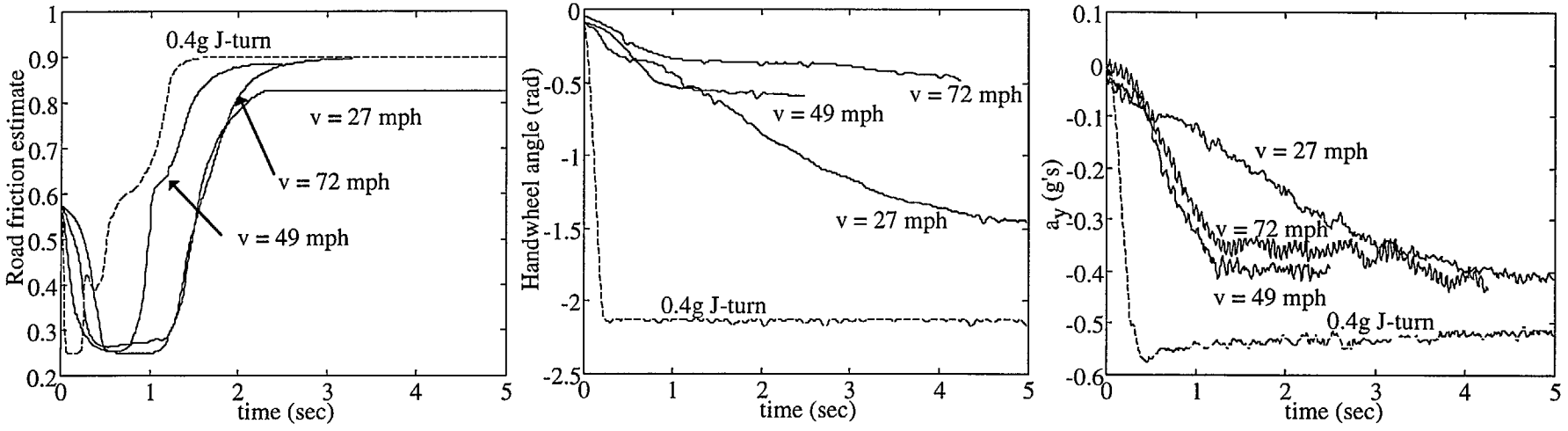
Road friction estimate
time (sec)
0.4g J-turn
v = 27 mph
v = 72 mph
v = 49 mph
Handwheel angle (rad)
time (sec)
v = 72 mph
v = 49 mph
v = 27 mph
0.4g J-turn
a_y (g's)
time (sec)
v = 27 mph
v = 72 mph
v = 49 mph
0.4g J-turn

Figure 19 20

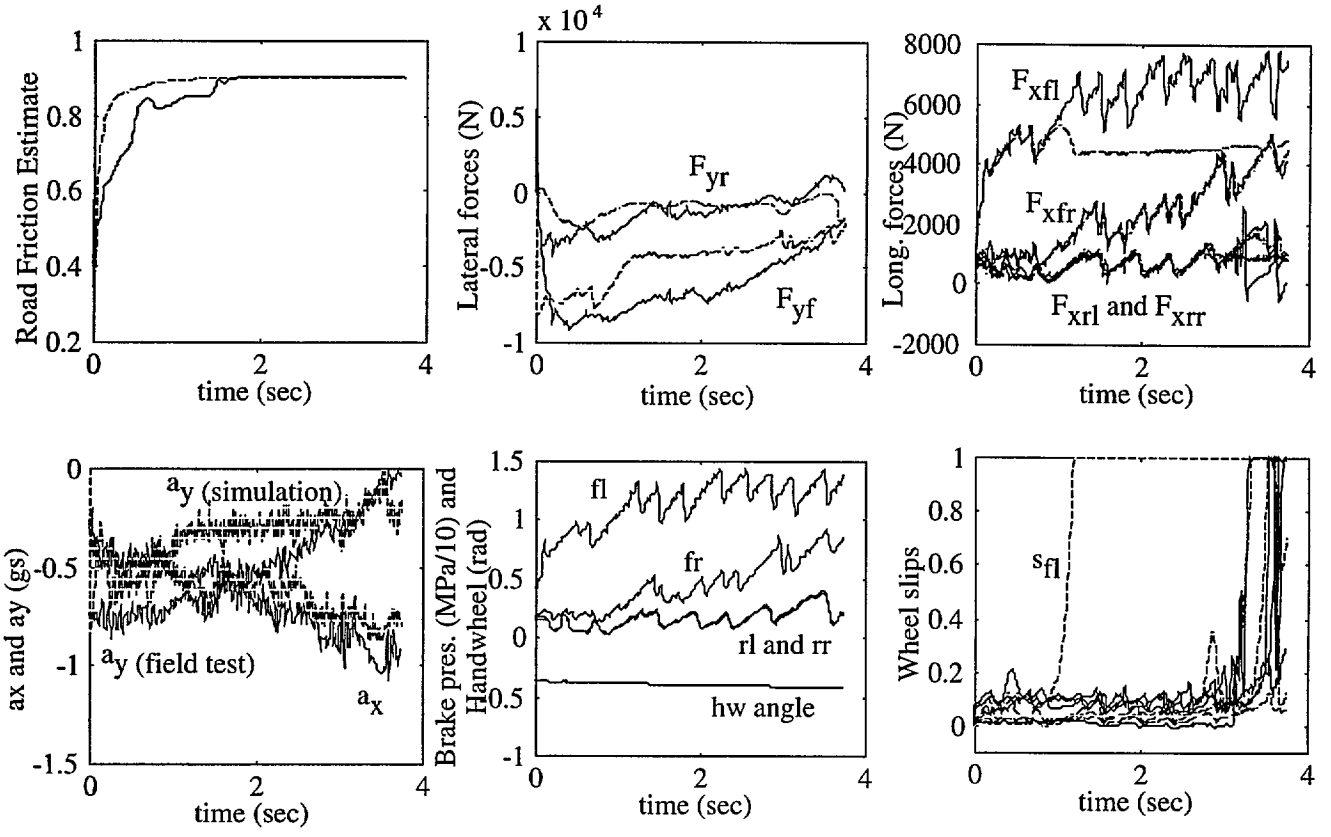
Road Friction Estimate
time (sec)
x 10^4
Lateral forces (N)
F_yr
F_yf
time (sec)
Long. forces (N)
F_xfl
F_xfr
F_xrl and F_xrr
time (sec)
ax and ay (gs)
a_y (simulation)
a_y (field test)
a_x
time (sec)
Brake pres. (MPa/10) and Handwheel (rad)
fl
fr
rl and rr
hw angle
time (sec)
Wheel slips
s_fl
time (sec)

Figure 21